Long-Term Efficiency of Horizontal Closed-Loop Geothermal Heat Exchangers for Stabilization of Permafrost beneath a Subarctic Lagoon

by

Amir Fatollahzadeh Gheisari

A Thesis submitted to the Faculty of Graduate Studies of The University of Manitoba in partial fulfilment of the requirements of the degree of

MASTER OF SCIENCE

Department of Civil Engineering

University of Manitoba

Winnipeg, Manitoba

Abstract

Wastewater treatment lagoons are practical and cost-effective systems for small municipalities to reduce nutrient and oxygen release into the environment. However, as they disrupt the natural soil temperatures, they initiate permafrost degradation and cause foundation instability and safety concerns in subarctic regions. In this thesis, the long-term effects of closed-loop horizontal geothermal heat exchangers (GHEs) on the stabilization of permafrost below a wastewater lagoon in northern Canada was studied. This research examined three different geometrical and operational parameters including pipe spacing, heat carrier inlet velocity and temperature which have the potential to impact the GHE performance in preserving ice-rich permafrost. Thaw settlement was addressed in this context. Also, a machine-learning algorithm was employed to predict unavailable future lagoon temperature based on the currently available weather data. The thesis concludes that the GHE with high-density polyethylene pipes can effectively mitigate and postpone the predicted permafrost thawing under a lagoon. However, under the projected climatic scenario, the GHE system even with every different selected operational parameters fails to eliminate thawing over its lifetime of 50 years. The heat exchangers' operational parameters substantially affect the permafrost thaw depth. Among all three studied parameters, the heat exchanger fluid temperature is the most influential parameter while the fluid inlet velocity only makes small differences in the thaw depth and thaw settlement.

Acknowledgement

I would like to thank my advisors, Dr. Pooneh Maghoul and Dr. Hartmut M. Holländer for sharing their wisdoms so kindly and patiently. I am extremely appreciative for their thoughtful mentoring and their unwavering support. Also, I would like to thank the KGS Group for providing data on the Ross River wastewater lagoon and Mr. Rob Sinclair, Ms. Maryam Saaly (KGS Group), and Hongwei Liu for their technical assistance and advice.

In addition, I acknowledge that this research was financially supported by Mitacs Accelerate Program and KGS Group.

Finally, I would like to thank my wife and my parents for their unconditional love and support during the last two years.

Contribution of Authors

Amir Fatollahzadeh Gheisari, Pooneh Maghoul, Hartmut M. Holländer, Rob Sinclair, Maryam Saaly. *Long-Term Efficiency of Horizontal Closed-Loop Geothermal Heat Exchangers for Stabilization of Permafrost beneath a Subarctic Lagoon.*

a) Amir Fatollahzadeh: Conceptualization, methodology, software, validation, investigation, data curation, writing-original draft, writing-review & editing
b) Pooneh Maghoul: Project administration, supervision, conceptualization, methodology, resources, writing-review & editing, funding acquisition
c) Hartmut M. Holländer: Project administration, supervision, conceptualization, methodology, resources, writing-review & editing, funding acquisition
d) Rob Sinclair: Field data, conceptualization, writing-review & editing
e) Maryam Saaly: Field data, writing-review & editing

Table of Contents

Abstract 2
Acknowledgement 3
Contribution of Authors 4
Table of Contents 5
List of Figures 7
List of Tables 8
List of Abbreviations 9
Nomenclature 10
Chapter 1: Introduction 11
1.1 Overview 11
1.2 Ground Source Geothermal System 11
1.3 Scope and Objectives 13
Chapter 2: Literature Review 14
2.1 Climate change adaptation strategies 14
2.2 Thermosiphons 14
2.3 GHE 15
Chapter 3: Methodology 17
3.1 Study area 17
3.2 Proposed GHE system specification 18
3.3 Conceptual model 19
3.4 Governing equations 21
3.4.1 Conductive heat transfer considering pore-water phase change: 21
3.4.2 Non-isothermal heat transfer from pipe flow: 23
3.4.3 Convective heat flux: 23
3.4.4 Convective heat flux at the ground surface in contact with the lagoon base: 24
3.4.5 Thaw Settlement 25
3.4.6 Lagoon base temperature from ambient air temperature 25
3.4.7 Prediction of lagoon base temperature 31
3.5 Numerical modelling and parameterization 32
3.5.1 Soil properties 32
3.5.2 Mesh 33
Chapter 4: Results and Discussions 34

4.1.1 Model validation 34
4.1.2 Effect of GHE system on permafrost preservation 35
4.1.3 The effect of operational parameters on the GHE performance 41
Chapter 5: Conclusion and Recommendations for Future Work 44
References 46

List of Figures

Fig. 1. a) Ross River, Yukon, b) Site plan of the Ross River wastewater lagoon and the borehole locations and c) Site stratigraphy and permafrost table 18

Fig. 2. Proposed geothermal concept 19

Fig. 3. Convective Heat flux, and adiabatic boundaries 19

Fig. 4 a) The whole domain, b) The repeated block of porous matrix and the embedded GHEs 21

Fig. 5. Average monthly air temperature in five wastewater locations, extracted from Environment and Climate Change Canada 26

Fig. 6. Shallow lake temperatures and the ANN simulation results 27

Fig. 7. Approximated lagoon temperature for different training approaches 30

Fig. 8. Projection of monthly mean air temperature at Faro for CanESM2 rcp8.5 pathways (Environment and Climate Change Canada, 2020). 31

Fig. 9. ANN predicted future monthly lagoon base temperature based on forcing data from CanESM2, rcp8.5. 31

Fig. 10. Domain mesh configuration 33

Fig. 11. Simulated and observed ground temperature profile for boreholes BH18-05 and BH18-06 on 24 May, 2019 34

Fig. 12. The defined cut lines and cut plane 35

Fig. 13. Maximum annual temperature (°C) in cut plane A-A without GHE system in six different years 37

Fig. 14. a) Temperature profile and permafrost thaw depth along the cut line A-A and b) lagoon and embankment settlement due to the permafrost thaw and with no embedded GHE system 38

Fig. 15. Maximum temperature (°C) in cut plane A-A equipped with the GHE system in six different years 40

Fig. 16. a) Temperature profile along cut line A-A at different times and b) lagoon and embankment settlements due to the permafrost thaw in the presense of embeded GHE system 41

Fig. 17. The effective radial distance of GHEs and the soil temperature (°C) profile of the cut plane B 42

List of Tables

Table. 1. Correlation coefficient (r) and RMSE of shallow lake temperatures and ANN simulated temperatures....29
Table. 2. Correlation factor and RMSE of the different training methods 30
Table. 3. Properties of the soils and fluids (Saaly et al., 2020; Bergman et al., 2017; Côté & Konrad, 2005) 32
Table. 4. Parameters used for heat transfer and isothermal pipe flow (Bergman et al., 2017; Tsytovich, 1985).....32
Table. 5. The effect of operational parameters on the permafrost thaw depth and settlement 42

List of Abbreviations

ANN	Artificial neural network
ACE	Air convection embankment
DVE	Duct ventilated system
FPCG	Fletcher-Powell conjugate gradient
GHE	Geothermal heat exchanger
GSGS	Ground source geothermal system
HDPE	High-density polyethylene
LM	Levenberg-Marquardt
MB	Manitoba
ON	Ontario
PRCG	Polak-Ribiére Conjugate Gradient
RBP	Resilient back propagation
SCG	Scaled conjugate gradient

Nomenclature

A	Pipe cross section area [m^2]
a	Curve control parameter [1/°C]
C_{app}	Apparent heat capacity [J/(kg. K)]
C_{pf}	Heat capacity of the fluid at constant pressure [J/kg. K]
d_h	Hydraulic diameter [m]
h	Thickness of the thawed/frozen layer [m]
$h_{conv(a)}$	Convective heat transfer coefficient of areas exposed to the ambient air
h_{int}	Film heat transfer coefficient on the inner pipe
$(h_Z)_{eff}$	Effective heat transfer coefficient
L	Characteristic length [m]
L_f	Latent heat per unit mass of water [kJ/kg]
n	Porosity
Nu_{int}	Pipe internal Nusselt number
P	Effective stress [MPa]
Pr_a	Prandtl number of air
q_a	Convective heat flux from air [W/m^2]
q_b	Geothermal heat flux [W/m^2]
q_l	Convective heat flux from lagoon [W/m^2]
Q	Heat source/sink [W/m^3]
r	Correlation factor
r_0	Pipe inner radius [m]
r_1	Pipe outer radius [m]
Re_L	Reynold's number
S	Total settlement [m]
T	Soil temperature [K]
t	Time [s]
T_a	Air temperature [°C]
T_0	Water freezing temperature [°C]
u	Fluid velocity [m/s]
u_a	Air velocity [m/s]
α	Thaw compression coefficient of frozen soil [1/MPa]
λ	Thermal conductivity of saturated frozen medium [W/(m. K)]
ρ	Density [kg/m^3]
γ_a	Air kinetic viscosity [m^2/s]
δ	Thaw strain of the frozen soils
Δm_v	Variation of volumetric compression coefficient of plastic frozen soil [1/MPa]
θ_{wr}	Residual unfrozen volumetric water content
θ_{w0}	Initial unfrozen water content

Chapter 1: Introduction

1.1 Overview

Permafrost is ground (soil, sediment, rock) that remains frozen for at least two consecutive years (National Research Council of Canada, 1988). Over the last 30 years, the mean temperature in the Arctic has risen at a rate of 0.54°C per decade, three times as fast as the rest of the globe (GISTEMP Team, 2021), resulting in permafrost thawing at an unprecedented rate. Permafrost degradation imposes severe threats to hydrology, ecology, health, environmental sustainability, and serviceability of infrastructure such as linear transportation infrastructures and building foundations.

Permafrost thawing can release a tremendous amount of carbon dioxide (CO_2) and methane (CH_4) into the atmosphere and exacerbate global warming. By 2100, it is estimated that 92 billion tons of trapped carbon in permafrost will be emitted into the atmosphere (Schuur et al., 2015). In Canada with 40 to 50% of the landscape underlain by frozen ground, permafrost destabilization has caused numerous issues in structures and buildings in subarctic regions. In the Northwest Territories alone, thawing permafrost underneath road embankments causes CA$51 million damage to public infrastructure every year (Northwest Territories Association of Communities, 2019). On Banks Island, Inuvik, a 60-fold increase in massive ground slumps was recorded from 1984 to 2013 (Lewkowicz & Way, 2019).

Wastewater lagoons have significant applications in the protection of public health and the environment through the prevention of nutrient release into the environment. They are popular in small communities of arctic and subarctic climates because of their simplicity, relatively low capital and operational costs and simple maintenance requirements (Oleszkiewicz & Sparling, 1987). However, under wastewater lagoons, permafrost thawing is highly likely because the lagoon base is much warmer than the ambient soil in cold seasons due to the chemical reactions in wastewater. Therefore, this heat source produces a heat flux which melts the permafrost resulting in a large settlement. In a wastewater lagoon in Yukon, Canada, for example, the long-term settlement due to permafrost thawing was predicted to be over 2 m (Tetra Tech, 2014).

1.2 Ground Source Geothermal System

Various field data measurements indicate that below a certain depth, the ground temperature remains relatively constant year-round. This is due to the high thermal inertia of the soil which diminishes the temperature variations at the ground surface as the depth increases (Florides & Kalogirou, 2007). Also, there is a time lag between the temperature fluctuations at the surface and in the ground, meaning that at a sufficient depth, the ground is always warmer than the ambient air in winter and colder than that in summer (Florides & Kalogirou, 2007).

Ground-source geothermal systems (GSGSs) is a clean technology that benefits from the rather constant ground temperature and have been in use for heating and cooling purposes of residential and commercial buildings over a decade. In addition to space conditioning, GSGSs are also used to provide domestic hot water for buildings, swimming pools and aquaculture. A Swiss patent issued in 1912 is the first known reference to geothermal systems (Chiasson, 2016; Spitler, 2005)

The geothermal energy is mainly harvested using two main systems: 1) shallow GSGSs which uses the low-temperature geothermal energy, found in depths of less than 250 m below the ground surface. This energy is mainly used for heating and cooling purposes in small to mid-sized residential buildings (Al-Khoury, 2011), 2) deep GSGSs which go down to a few kilometres below the ground surface where the ground temperature has a very high temperature, usually 150°C or higher (Al-Khoury, 2011). This energy is harvested and then used for higher energy demands (e.g. heating demand of Aachen University, Germany, (Dijkshoorn et al., 2013))

Three main components of almost all GSGSs include i) Earth as a heat source and the buried connected pipes (known as heat exchangers) in which a fluid circulates and absorbs heat from or releases heat to the ground, depending on whether the soil is colder or warmer than the ambient air ii) Heat pump subsystem that removes the heat from the fluid and transfers it to the air or water in the building with a reverse process for the cooling. iii) Heat distribution subsystem to distribute heated or cooled air from the geothermal heat pump in the building (Self et al., 2013). A brief description of each component is presented as follows:

Geothermal heat exchangers

One of the most crucial components of the GSGS systems which determines the initial installation cost of the entire system is geothermal heat exchanger (GHE) (Yoon et al., 2015). GHEs consist of pipes, buried in the subsurface that exploit the constant heat of the ground, which is warmer than the ambient air in winter and cooler during summer. The heat transfer between the heat carrier and ground takes place through the convection process. The fluid is then carried to the heat pumps where it harvests the transferred energy for heating or cooling purposes.

Heat pumps

Heat pumps operate using electricity to remove the thermal energy from the circulated fluid, compress it and then transfer it to the building (Omer, 2008). For cooling, the heat is added to the ground in a reverse cycle. Heat pumps are one of the most energy-efficient methods of domestic and industrial heating. A typical heat pump only requires 100 kWh of electricity power to turn 200 kWh of freely available ground heat to 300 kWh of useful heat (Omer, 2008). Heat pumps also have a very low carbon footprint, less than half than that of electric, oil, and gas heat production, making it an environmental-friendly technology.

Heat distribution system

The heat distribution system delivers the thermal heat extracted by GHEs to the space. Two common types of distribution systems are water to air and water to water (Self et al., 2013). In the water to air system, the transport medium within the space is air, where the warm air coming from the condenser unit passes through the building using HVAC systems and air vents. In water to water system (commonly known as hydronic system), on the other hand, water or a similar fluid is pumped through the condenser unit. The warm water is then distributed around the building delivering heat using in-floor radiant heaters, radiators or localized air coils (Self et al., 2013).

1.3 Scope and Objectives

The main objective of this research is to investigate the feasibility of using GHE systems and long-term efficiency of such systems for preserving permafrost against thawing under different climate change scenarios. This main objective has three sub-objectives which are:

1. Permafrost degradation due to the climatic conditions and the maximum expected thaw settlement
2. The effect of GHEs on the permafrost preservation
3. The effect of operational parameters of the GHE systems on the permafrost thaw depth and settlement

Chapter 2: Literature Review

2.1 Climate change adaptation strategies

Over the last few decades, climate change adaptation strategies and mitigation solutions have been developed to overcome the adverse effect of climate warming on northern infrastructure. These techniques can be generally categorized into three main groups: (i) limiting the heat transfer from the atmosphere into permafrost, (ii) extracting heat to cool permafrost, and (iii) reinforcing the infrastructure against settlement (Doré et al., 2016). Group (i) technique attempts to reduce absorbed heat transfer from solar radiation in summer as one of the prominent heat sources. Examples of this technique are elevating the embankment level or placing lower heat conductive material such as sand or polystyrene insulation beneath the embankment (Doré et al., 2016; Wen et al., 2008; Zhang et al., 2005). Group(ii), known as heat extraction method, aims to remove heat from the system and lessen the temperature of permafrost-affected soil. There is a wide variety of techniques used to extract the ground heat such as heat draining method, duct ventilated embankment (DVE), air convection embankment (ACE) and thermosiphons. Group(iii), referred to as the reinforcement method, usually concerns improvements in the mechanical stability of the embankment to resist faulting or localized subsidence when preventing permafrost from thawing is not practical (Doré et al., 2016). In the following subsections, thermosiphons as the most common permafrost stabilization method and GHE as an alternative in cooling the permafrost are described in more details.

2.2 Thermosiphons

From the wide range of permafrost stabilization methods, thermosiphons have been the most-widely used due to their simple structure, high efficiency and low fabrication costs (Jiao et al., 2008) . This technique is based on natural convection and so, no external energy is used. Despite all advantages of thermosiphons, there are some drawbacks attached to this system. Primarily, the performance of thermosiphon heavily depends on the ambient temperatures. In summer, the system is unable to provide heat and can only store the cold by using the thermal insulation part. Thermosiphons need to have an airtight vacuum so leaks and detecting them can impose extra cost of repair and inspection (e.g. Inuvik hospital, Northwest Territories (Holubec, 2008)). Incidents or vandalisms are other issues of thermosiphons due to their exposure above the ground. To overcome its shortcomings, this system is sometimes coupled with other techniques such as the thermal insulation layer (Zhi et al., 2005) and heat pumps (Huang et al., 2005). However, this increases the construction and operational cost and complicates the understanding of the interactional performance of the thermosiphon.

2.3 GHE

GHEs are the part of GSGS system consisting of buried pipes which thermally interact with the adjacent ground. There are two types of heat exchangers: open loop and closed-loop (Florides & Kalogirou, 2007). In the open loop system, the groundwater is used as the heat carrier fluid and is directly carried to the heat pump. In a closed-loop system, ground heat is transferred with the aid of a circulated heat carrier medium (Florides et al., 2013).

The heat exchangers are made of an extremely durable material yet thermally conductive that allows heat to pass through efficiently. HDPE pipes are one of the most widely used heat exchangers usually guaranteed for as much as 50 years (Florides et al., 2013). GHEs are also classified into vertical and horizontal loop systems, although hybrid systems such as inclined or pile systems are available as well (Lamarche, 2019). While vertical borehole systems are the most popular GSGS systems in Europe, in North America, horizontal systems are largely used due to the land availability and lower investment costs (Gheysari et al., 2021).

Numerous researchers have studied GHEs in the last few decades. Claesson and Dunand (1983) were the first who presented a steady-state analytical formulation for the pipe system. They concluded that the fluid temperature and the heat flux exponentially decay along the pipes. The decay rate is governed by the thermal characteristic length of the system, pertaining to its thermal resistance.

There are two major analytical methods to determine the temperature distribution around the pipes, namely the Kalvin Line Source Theory and the Cylindrical Source Theory. However, both theories are merely able to model a symmetrical soil temperature distribution around the pipes (Kayaci & Demir, 2018). Mei (1991) modified the Kalvin Line Source model by including the effect of pipe material, liquid properties, and seasonal ground temperature variation. Gauthier et al. (1997) simulated a fully three-dimensional model and validated the results with an experimental analysis. They reported that the heat transfer in the pipes is in the axial direction, but coupled with the ground temperature field adjacent to the pipes. Kayaci et al. (2015) numerically analysed the long-term soil temperature distribution and investigated the effect of the surface condition on it. Cai et al. (2019) numerically studied the long-term performance of deep boreholes and experimentally verified the results.

GHE for stabilizing permafrost

Geothermal heat exchangers (GHEs) with a similar function to thermosiphons in the extracting heat have been traditionally used for heat energy supply and heating/cooling demand of buildings. However, their effects on permafrost stabilization have rarely been studied. Fontaine et al. (2011) presented a new analytical model to study the effect of a spiral-shaped horizontal ground heat exchanger on permafrost stabilization. They also investigated the effect of pipe length, depth and spacing on heat extraction rate and the ground temperature. However, their model overestimated the summer ground temperature and thaw

depth. Besides, only a short-term (5 years) analysis was carried out and the long-term performance of the GHE system was not investigated. Lamarche (2019) modelled GHEs and investigated the seasonal temperature variation of soil. The model used sub-zero temperatures for permafrost regions; however, pore water phase change was not considered. Similar to Fontaine et al. (2011), the long-term performance of the system was not explored. Bayasan et al. (2008) developed a statistical modelling for estimating the capacity of permafrost beds and used vertical GHEs to lower the permafrost temperatures. They concluded that GHEs are highly beneficial in increasing the stability of permafrost beds so this system can be an excellent alternative to the energy-consuming and expensive refrigerant equipment in the stabilization of the transmission lines and building foundations. However, in their model they used random climatic parameters and a highly complex probabilistic method that resulted in more uncertainty levels. Similarly, in their research, they only studied the effect of GHEs for a 6-months period and the long-time performance of the system was not investigated.

Chapter 3: Methodology

3.1 Study area

This research was carried out on a freeze-back system at the Ross River's wastewater lagoon in a permafrost rich area, Yukon, Canada (Fig.1a). Due to the 3 m excavation for the construction of the wastewater lagoon, the underlying permafrost was exposed to the downward heat flux from the lagoon base. The heat is due to the solar radiation into the wastewater in the lagoon, leading the lagoon to maintain a temperature above the freezing temperature all year-round. Besides, the lagoon construction impeded seasonal frost within the upper soil.

Ross River is a community of roughly 350 people located approximately 60 km east of the Town of Faro and 300 km north of Whitehorse, Yukon. Yukon is divided into three permafrost zones with different permafrost coverage ratios: continuous (90-100%), extensive discontinuous (50-90%), and sporadic (10-50%) (Heginbottom et al., 1995). The Ross River community is located within the zone of extensive discontinuous and mostly warm permafrost.

A geotechnical investigation (Tetra Tech, 2014) indicated that the site stratigraphy consists of approximately 2 to 3 m of sandy gravel above a 3.2 to 4 m clayey silt layer. Ice lensing up to 20 mm thick had been identified within the clayey silt. The presence of this ice lensing was a significant design consideration, as the lagoon acts as a heat source, thereby changing the thermal regime of the permafrost site. According to the data acquired from two boreholes of CH18-05 and CH18-06 (Fig.1b), the average observed permafrost layer started at 8 m below the original ground level and 5 m below the lagoon base, and it extended to 22 m in depth (Fig.1c).

The present wastewater lagoon for the community is located to the west of the community, approximately 700 m south of the Pelly River. The lagoon system was constructed in fall 2017 and consisted of two cells; a primary cell and a secondary cell with the base dimensions of 75 m × 15 m and 75 m × 35 m, respectively, as well as a tankage for solids removal prior to the lagoon and a sludge drying bed for sludge treatment. The lagoon base was placed 3 m below the original ground level through excavation, and the maximum lagoon depth was 3 m, as well. The wastewater lagoon system was designed for the wastewater production per capita of 110 L/day/person, the annual wastewater production of 17000 m^3/year and 10-month storage volume of 14000 m^3/year (Sinclair & Theissen 2014).

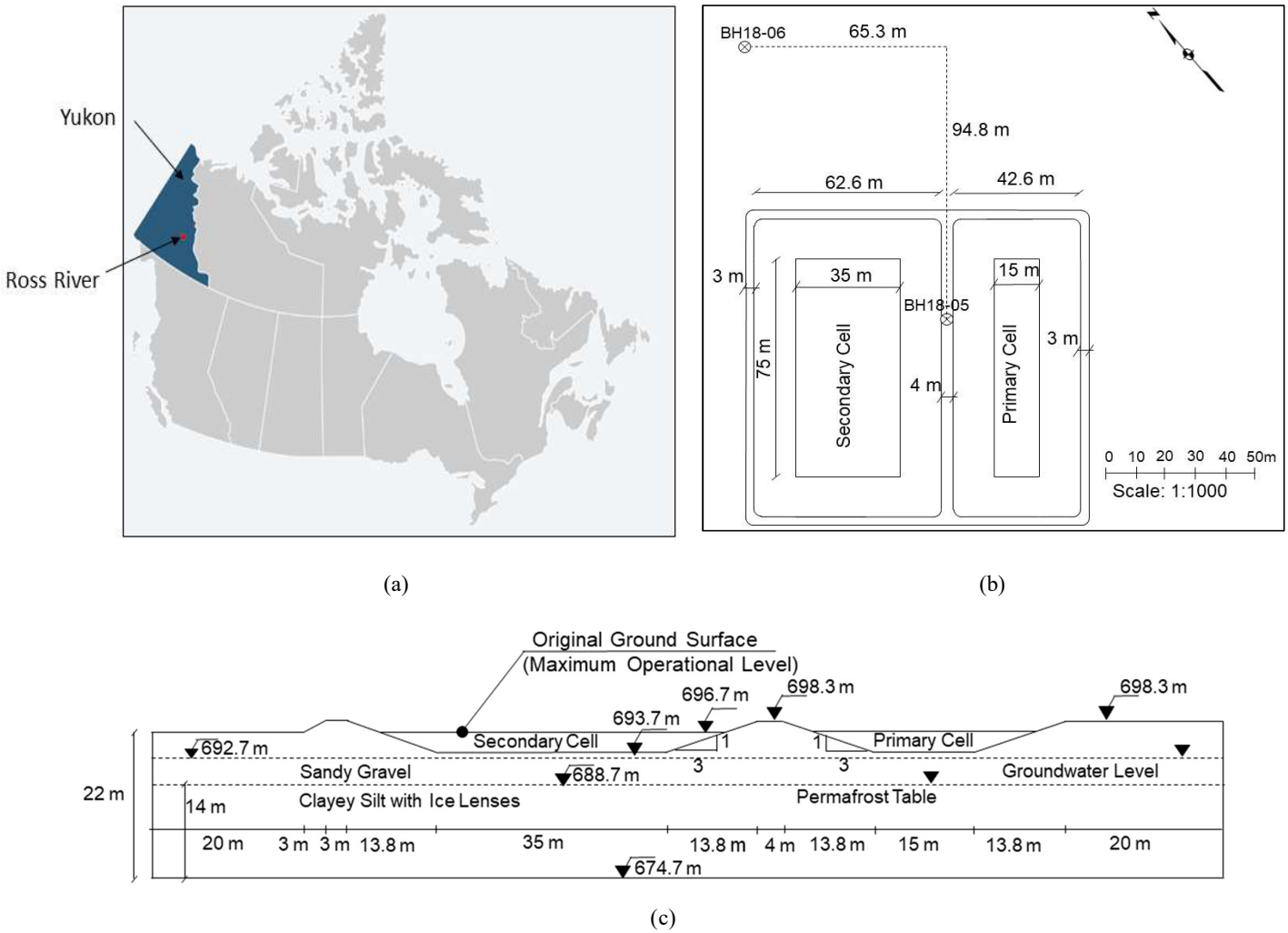

Fig. 1. a) Ross River, Yukon, b) Site plan of the Ross River wastewater lagoon and the borehole locations and c) Site stratigraphy and permafrost table

3.2 Proposed GHE system specification

The modelled GHE system (Fig.2a) consisted of seventy-eight HDPE pipes, each 50 mm in diameter and 45 m and 70 m long, which were placed under the primary and secondary cells, respectively. The pipes were placed 2 m apart horizontally and 1.5 m below the lagoon's base (4.5 m from the original ground level), through which cold fluid continuously circulated to transfer cold into the surrounding soil. The central header was employed to distribute the heat carrier fluid flow equally and maintain the cold temperature in all the heat exchangers inlet points (Fig.2). The heat carrier fluid was a 30% ethanol-water blend.

Although a thermal insulation layer could considerably decrease the lagoon's heat injection, it was not considered in the present study since no insulation layer was implemented in the actual design of the Ross River Lagoon (Saaly et al., 2020). Also, due to the significant constant heat flux of the wastewater lagoon and high cooling demand for permafrost stabilization, the GHE system operated all year round, so seasonal balancing was not studied.

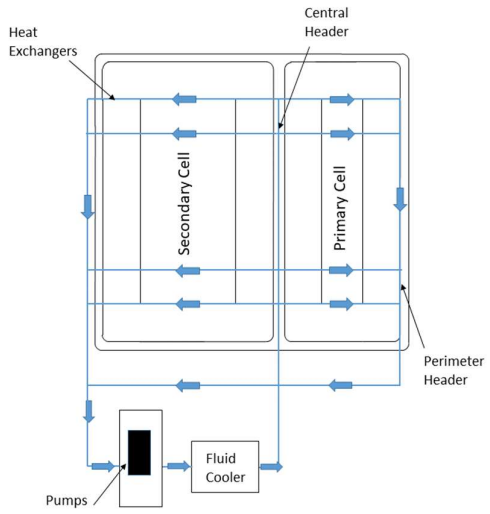

Fig. 2. Proposed geothermal concept

3.3 Conceptual model

The domain's top boundary was in contact with the surrounding air and the lagoon base. Due to the exposure to the ambient air, a forced convective heat flux (q_a) was assigned to the parts of the top boundary exposed to the air. The boundary condition at the interface between the lagoon base and the soil is also defined by a convective heat flux (q_l) (Saaly, et al., 2020). The way q_a and q_l are calculated is thoroughly explained in the governing equation section. In addition, a constant upward heat flux (q_b) is applied to the bottom of the domain to represent the geothermal heat flux that exists at the site. The sides of the domain were defined as adiabatic boundaries shown in Fig.3. It should be noted that the heat fluxes from solar radiation and snow fall (sensible heat flux) were neglected due to their negligible effects compared with the lagoon and ambient heat flux.

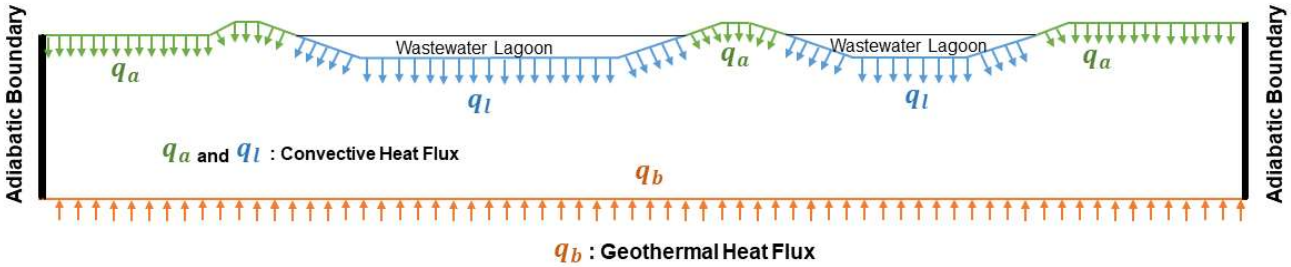

Fig. 3. Convective Heat flux, and adiabatic boundaries

A series of 3D multi-physics finite element (FE) simulations of a GHE system including thermal analysis of heat exchangers and the soil body by considering the porous nature of soils and seasonal freeze-thaw cycles was conducted in COMSOL Multiphysics v5.4 (Fig.4a). Using the symmetry in the layout of the HDPE pipes, only one repeated block of the soil domain with the embedded heat exchangers was considered

to decrease the computational time (Fig.4b). In numerical modelling, the side boundaries usually create unwanted results which can interfere with the result of the rest of the model and cause erroneous outputs. To avoid this problem, the block width was chosen four times the horizontal distance between two adjacent heat exchangers. Since the pipe spacing varied for each simulation, the block width varied correspondingly. The analysis was divided into two subsections: in the first part, the effect of the GHE system on preserving permafrost was investigated. For this purpose, the model was initially simulated without the GHE system to determine how the permafrost beneath the wastewater lagoon reacts to climatic heat fluxes and lagoon temperature variation. Consequently, the simulations were carried out with an operational GHE system. The GHE parameters such as pipe spacing, heat carrier inlet velocity, and temperature affect the system performance. The initial values selected were 2 m, 0.4 m/s and -10 °C, for pipe spacing, heat carrier inlet velocity and temperature, respectively. In the second section, the effect of the above-mentioned operational parameters on the long-term performance of the GHE system was investigated by varying these parameters. Different pipe spacing, heat exchanger velocities and temperatures were modelled to understand their effects on the system efficiency. For this purpose, 4 different pipe spacings (1.0, 1.5, 2.0, and 2.5 m), 3 heat exchanger inlet velocities (0.2, 0.4, and 0.6 m/s) and 4 heat exchanger inlet temperatures (-5, -10, -15, and -20°C) were tested. To detect the independent effect of each operational parameter on the system performance, only the parameter of interest varied while the two other parameters were considered constant at their lowest/highest values (0.2 m/s and -5°C for the heat exchanger inlet velocity and temperature/2.5 m for the pipe spacing). The simulation was performed for 50 years with one-month time intervals to evaluate the sustainability of the GHE system proposed in this study.

Surface Energy Balance (SEB), as one of the most realistic methods, has been conventionally used to calculate the ground surface temperatures in contact with air. The common approach of the freezing and thawing n-factor is a method to calculate the ground surface temperature based on the air temperature. However, the complexity and high uncertainty level in the future trend of climate parameters in the former and over the simplified assumption of the latter are the attached drawbacks of both methods.

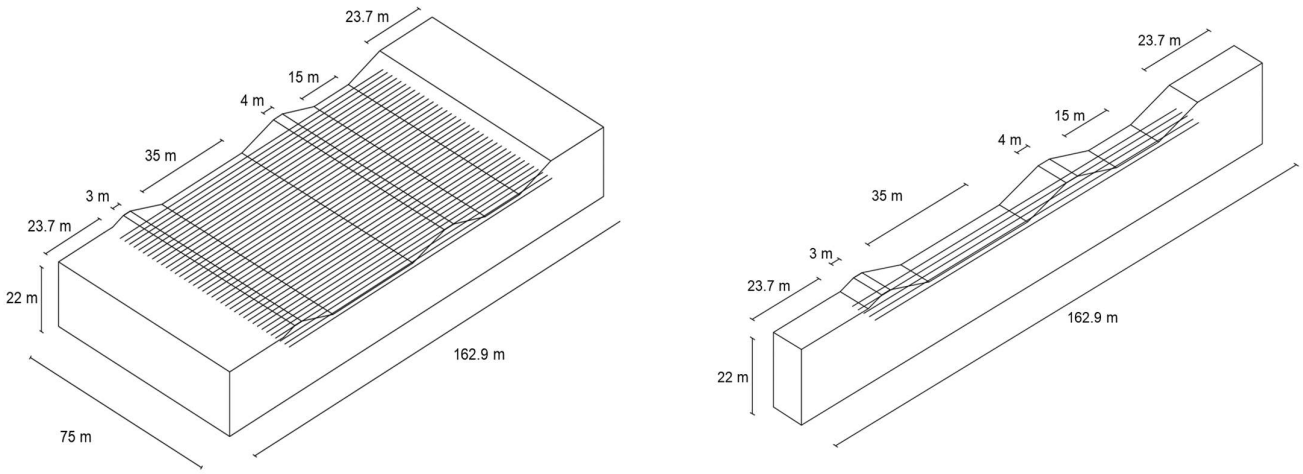

(a) (b)

Fig. 4 a) The whole domain, b) The repeated block of porous matrix and the embedded GHEs

3.4 Governing equations

The study of the effectiveness of a GHE system on the stabilization of a thawing permafrost layer requires different physics: 1) the porous nature of soil and its temperature-dependent physical characteristics, 2) heat transfer mechanism in porous soil, and 3) pipe flow and heat exchange through its walls. The governing equations of each physic are presented in the following sections:

3.4.1 Conductive heat transfer considering pore-water phase change:

The heat transfer formulation in the porous media is similar to general heat transfer formulation, except that the effective heat capacity and the effective thermal conductivity are introduced to account for porosity. When a material's phase changes, for instance from solid to liquid, energy is added to the particles defined as the latent heat. Therefore, instead of a temperature rise, the energy alters the material's micro structure. According to Michalowski and Zhu (2004), the governing equation for transient heat conduction in the soil by considering the latent heat of pore-water can be described as (Liu et al., 2019):

$$(C_{app})\frac{\partial T}{\partial t} + \nabla \bullet q = Q \tag{1}$$

where T [K] is the soil temperature, Q [W/m^3] is the heat source/sink, $\nabla = (\frac{\partial}{\partial x}, \frac{\partial}{\partial y}, \frac{\partial}{\partial z})$ is the gradient vector and t [s] is time, and q [W/m^2] is the conductive heat flux as defined by Fourier's law:

$$q = \lambda \nabla T \tag{2}$$

where λ [W/(m. K)] is the thermal conductivity of the saturated frozen medium.

The first term in Eq.1 is defined as the apparent heat capacity [J/(kg. K)], expressed as:

$$C_{app} = \frac{1}{\rho}(\rho_{ph} C_{ph} - L_f \rho_i \frac{\partial \theta_i}{\partial t}) \quad (3)$$

here L_f [kJ/kg] is the latent heat per unit mass of water, ρ [m/kg^3] is the bulk density of the porous medium, ρ_i [m/kg^3] is the density of ice and θ_i is the volumetric fraction of ice in pores.

Also, $\rho_{ph} C_{ph}$ [J/(m^3. K)] denotes the volumetric heat capacity of the soil mixture which can be calculated by the sum of the volumetric heat capacity (ρC) of each constituent of the saturated freezing medium (solid skeleton, water, and ice) multiplied by its volumetric fraction (θ) as follows :

$$\rho_{ph} C_{ph} = \rho_s C_s \theta_s + \rho_w C_w \theta_w + \rho_i C_i \theta_i \quad (4)$$

where s, w, and i denote solid skeleton, water, and ice, respectively. Similarly, thermal conductivity (λ) and the bulk density (ρ) of the saturated frozen soil mixture can be defined as Eq.5 and 6, respectively:

$$\lambda = \rho_s \theta_s \lambda_s + \rho_w \theta_w \lambda_w + \rho_i \theta_i \lambda_i \quad (5)$$

$$\rho = \rho_s \theta_s + \rho_w \theta_w + \rho_i \theta_i \quad (6)$$

where ρ_s , ρ_w , ρ_i and λ_s , λ_w , λ_i are the density and thermal conductivity of soil, water and ice, respectively.

When the soil temperature drops below the freezing point, water inside pores starts freezing although some portion of pore water remains liquid even below the freezing temperature (Saaly et al., 2019). This affects the effective thermal properties of the soil as θ_i change. The below empirical relation (Michalowski & Zhu, 2004) estimates the unfrozen water content fraction of the frozen soil (θ_{uw}):

$$\theta_{uw} = \theta_{wr} + (\theta_{wo} - \theta_{wr})\ e^{a\ (T - T_0)} \quad (7)$$

where θ_{wr} is the residual unfrozen volumetric water content, θ_{w0} is the initial unfrozen water content, a [1/°C] is a parameter that controls the curvature and T_0 is the freezing temperature and is considered 0°C. Also, the volumetric fraction of ice can be calculated as:

$$\theta_i = n - \frac{\rho_s}{\rho_w}(1 - n)\ \theta_{uw} \quad (8)$$

where n is the soil porosity.

3.4.2 Non-isothermal heat transfer from pipe flow:

The heat exchangers thermally interact with the surrounding soil through the heat conduction mechanism due to the thermal gradient. In order to couple the heat transfer in a solid with the heat transfer from the pipe flow, the following differential energy equation is required (Dacquay et al., 2020):

$$\rho A C_{app} \frac{\partial T}{\partial t} + \rho_f A C_{pf} u.\nabla T = \nabla A \lambda_f \nabla T + \frac{\rho}{2 d_h} |u|^3 + Q_{wall} \tag{9}$$

where A [m^2] is pipe cross section area, C_{pf} [J/kg. K] is the heat capacity of the fluid at constant pressure, T [K] and λ_f [W/(m· K)] are the fluid temperature and thermal conductivity, d_h [m] is the hydraulic diameter and u [m/s] is the fluid velocity.

Also, Q_{wall} [W/m^3] is the external heat source/sink term through the pipe wall and is formulated as follows:

$$Q_{wall} = (h_Z)_{eff} (\ T_{ext} - T) \tag{10}$$

T_{ext} [°C] is the external temperature outside of the pipe and $(h_Z)_{eff}$ is the effective heat transfer coefficient and for a circular tube is calculated as (Bergman et al., 2017):

$$(h_Z)_{eff} = \frac{2\pi}{\frac{1}{Z_0\ h_{int}} + \ln(\frac{r_1}{r_0}) / \lambda_f} \tag{11}$$

such that r_0 and r_1 are inner and outer pipe radius [m], respectively. λ_f [W/m. K] is the thermal conductivity of the pipe wall and h_{int} [W/m^2.K] is the film heat transfer coefficient on the inner pipe, calculated as:

$$h_{int} = Nu_{int} \frac{\lambda_w}{d_h} \tag{12}$$

where Nu_{int} is the internal Nusselt number taken as 3.66 for the laminar flow regime and d_h is the hydraulic diameter.

3.4.3 Convective heat flux:

The soil temperature near the ground surface is heavily dependent on climatic temperature changes (Saaly et al., 2020). To model the seasonal temperature variation on the soil temperature, a convective heat flux was assigned to the area of the top domain boundary with a contact to the ambient air:

$$Heat\ Flux: q_a(t) = h_{conv(a)}(T_a(t) - T(t)) \quad (13)$$

where $h_{conv(a)}$ [W/m^2°C] is the convection heat transfer coefficient for the domain area exposed to the ambient air. T [°C] is the ground surface temperature (calculated in each time step) and T_a [°C] is the air temperature at the ground surface, available in Environment and Climate Change Canada, 2020.

The convection heat transfer coefficient, h_{conv}, depends mainly on conditions on the boundary layer (Bergman et al., 2017). The average convective heat transfer coefficient for the external forced convection on a horizontal surface can be calculated as follows (Welty et al., 2020):

$$h = 2\frac{\lambda}{L}\begin{cases} \dfrac{0.3387 P_r^{\frac{1}{3}} Re_L^{\frac{1}{2}}}{\left(1 + (\frac{0.0468}{P_r})^{\frac{2}{3}}\right)^{\frac{1}{4}}} & if\ Re_L < 5.10^5 \\ Pr^{\frac{1}{3}}\left(0.037 Re_L^{\frac{4}{5}} - 871\right) & if\ Re_L > 5.10^5 \end{cases} \quad (14)$$

where λ_a is the thermal conductivity of air (0.02 [W/m. K], (Liu et al., 2019)). Pr_a is the Prandtl number of air (equal to 0.7, (Dacquay et al., 2020)), defined as the ratio of thermal diffusivity to viscosity. Re_L is Reynold's number based on the characteristic length L, calculated as follows:

$$\mathrm{Re}_L = \frac{u_a.L}{\gamma} \quad (15)$$

where u_a [m/s] is the air flow velocity and γ_a is the kinematic viscosity of air (1.3×10^{-5} [m^2/s]).

3.4.4 Convective heat flux at the ground surface in contact with the lagoon base:

The boundary conditions at the interface between the lagoon base and the ground surface are also defined by a convective heat flux, formulated as follows:

$$q_l(t) = h_{conv(l)}(T_l(t) - T(t)) \quad (16)$$

where T_l (°C) is the lagoon temperature. In this study, the concrete material is placed between wastewater and soil. The h value for the concrete between wastewater and soil does not exist in the literature, so in this study, the h value was quantified numerically using finite element analysis. For this purpose, a 3-D model was set up in COMSOL Multiphysics, where an 8-cm concrete layer (real value from the Ross River Lagoon) was placed above the soil and beneath the wastewater to calculate the heat transfer coefficient.

The result of the stationary heat transfer analysis yielded 4.0 and 5.0 [W/m^2°C], for the heat transfer coefficient of the inclined sides and horizontal bottom boundary, respectively.

3.4.5 Thaw Settlement

Numerous research studies have been conducted for estimating the settlement of foundation soil in permafrost regions (Gregersen et al., 1985; Wu et al., 1983; Zhang et al., 2016) and some theories have been developed and introduced such as creep and thaw consolidation of frozen soils (Ladanyi & Andersland, 2004; Vyalov, 2005). However, practical implementations of these theories are technically difficult, especially when the ground temperature variation is complex (Zhang et al., 2016). In this study, a simplified widely accepted method proposed by Tsytovich (1985) was used to estimate the thaw settlement. In this method, the settlement of the foundation soil consists of thaw settlement of permafrost soil by self-weight and applied load, as well as compression of frozen soil defined as:

$$S = S_1 + S_2 + S_3 = \sum_{i=1}^{n} \delta_i .\ h_i + \sum_{i=1}^{n} \alpha_i .\ P_i .\ h_i + \sum_{j=1}^{m} \Delta m_v .\ P_j .\ h_j \qquad (17)$$

where S [m] is the total settlement of the foundation soil, S_1 is the thaw settlement of the frozen soils due to the self-weight, S_2 is the thaw compression of the frozen soil due to the applied load, and S_3 is compression of the plastic frozen soils induced by the applied load. δ is the thaw strain of the frozen soils, h [m] is the thickness of the thawed/frozen layer, α [1/MPa] is the thaw compression coefficient of frozen soils, P [MPa] is the effective stress applied to the soil domain and Δm_v [1/MPa] is the variation of volumetric compression coefficient of plastic frozen soil due to the temperature rise. Also, i and j denote the number of thawed and frozen soil layers, respectively.

3.4.6 Lagoon base temperature from ambient air temperature

The lagoon base temperature and its heat leakage play the primary role in melting the ice lenses in permafrost thawing. However, historical temperatures of the Ross River wastewater lagoon base were not available due to its short operational time. Also, to study the long-term efficiency of the geothermal system, the predicted future lagoon base temperatures are needed while they do not exist either.

To overcome this problem, a data-driven Artificial Neural Network (ANN) algorithm was used for function approximation to describe the relationship between the lagoon base temperature and the ambient air temperature. Air temperature is available for a nearby weather station (station Faro) and future climates (until 2100) by Environment and Climate Change Canada (2020). Therefore, the ANN used the projected air temperatures as the input data and approximated the future lagoon base temperature. For this purpose, lagoon base temperatures in areas with similar freezing seasons to the Yukon area were needed for ANN training, validation and testing processes. However, there are limited recordings of historical lagoon base temperatures in cold regions because lagoon operators are not obliged to monitor the temperature of the lagoons in most countries.

As an alternative, shallow lakes with depths close to the depth of the Ross River wastewater lagoon (3 m) were identified to have temperatures similar to the lagoon base temperatures as they both vary seasonally from near ambient air temperature in late summer to just above 0°C in late winter. Thus, two sets of data including the base temperature of the few existing lagoons and their nearby shallow lakes' temperature were studied to validate this assumption. For this purpose, four wastewater lagoons in similar climatic zones to Yukon with the depth of 2 to 5 m along with 5 nearby shallow lakes (within 500 km distance) for each lagoon were studied. These lagoons are in Lorette (MB), Niverville (MB), Portage la Prairie (MB), and Guelph (ON) and their monthly average base temperatures are available in the literature (Bemister, 1978; Hart & Halden, 2020; Smyth et al., 2018). The average monthly air temperature of these locations (Fig.5) shows a 5-month freezing period for all four locations, the same number as Faro, the nearest metrological station to Ross River.

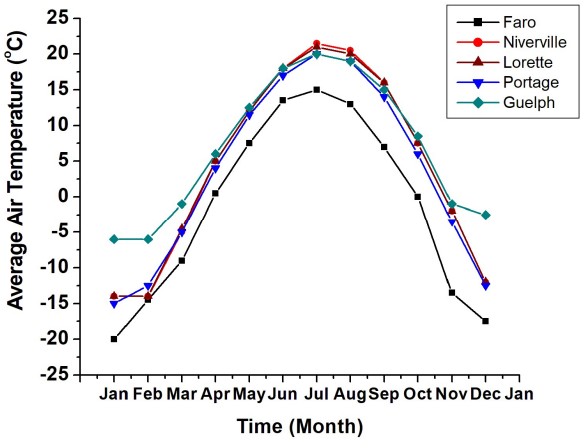

Fig. 5. Average monthly air temperature in five wastewater locations, extracted from Environment and Climate Change Canada

Due to the inadequate existing lagoon base temperature to feed the ANN, the temperatures of the nearby shallow lakes (within 500 km) were examined to see if their monthly water temperatures are close to wastewater lagoon base temperatures. For this purpose, for each of the four wastewater lagoons, five lakes all within 500 km to the lagoon location were chosen. Most of the selected lakes had an average depth of 4 to 6 m. Although the average depth of a few chosen lakes (3 out of 20) exceeds this range, the location in which their temperature was measured is in the range of 4 to 6 m. The selected lakes were Lake Winnipeg, Victoria Lake, Hecla Lake, Alberts Lake and Balsam Lake for the Lorette Lagoon, Gimli Beach, Grand Beach, Delta Beach, Grand Maraise and York Factory for the Niverville Lagoon, Walker Lake, Playground Lake, Eleanor Lake, Dorothy Lake and Cross Lake for the Portage la Prairie Lagoon and Burlington Lake, Churry Beach, Cobourg Lake, Rideau Lake and Little Channel Lake for the Guelph Lagoon.

The results revealed a considerable difference between the four studied lagoons' base temperature and their nearby shallow lakes (Fig.6). This difference was more significant in April through July in Lorette and Niverville Lagoon and March through June in Portage la Prairie and Guelph lagoon. The maximum

difference in the lagoon base and shallow lake temperature was 6.7, 19.1, 10.5, and 8.8 ℃ in the Lorette, Niverville, Portage la Prairie and Guelph.

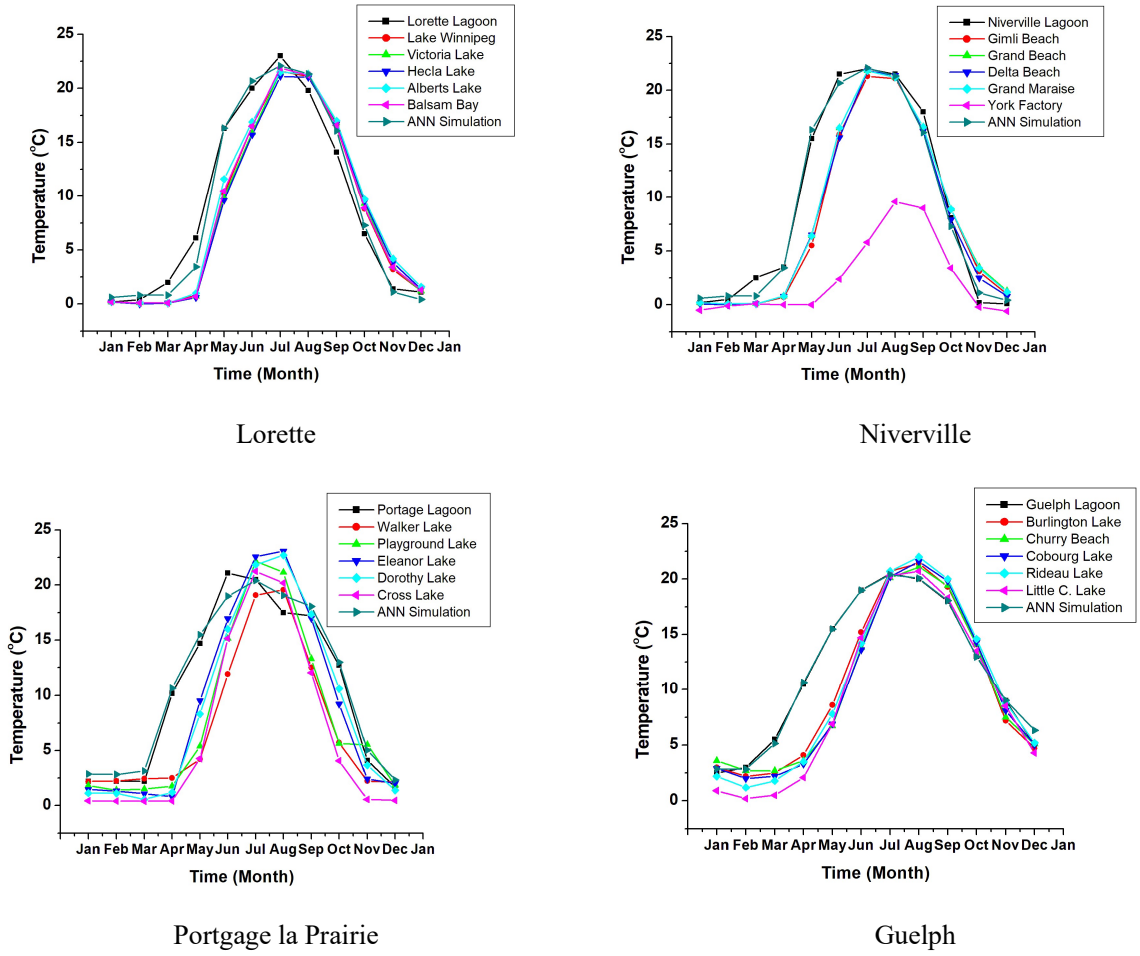

Fig. 6. Shallow lake temperatures and the ANN simulation results

To minimize the difference between the lagoon base temperature and the shallow lake temperature, a feed-forward back-propagation ANN algorithm was used such that the shallow lake temperatures first go through the network, get processed, and then are used as the simulated lagoon base temperatures. 288 data points and10 hidden layers were used where 80%, 10%, and 10% of data were allocated to training, validation and testing process, respectively. Also, Levenberg-Marquardt (LM) was used as the ANN training method at this stage (Gheysari et al., 2021).

To see the discrepancy between the nearby shallow lake temperatures and ANN simulated results with the lagoon temperatures, two statistical criteria were introduced to evaluate the error that exists between the data sets.

The first criterion is the correlation coefficient (r), a number that ranges from 0 to 1 and is defined as:

$$r = \sqrt{\frac{S_t - S_r}{S_t}} \tag{18}$$

$$S_t = \sum_{i=1}^{n} (y_{real} - \bar{y})^2 \tag{19}$$

$$S_r = \sum_{i=1}^{n} (y_{real} - y_{approx.})^2 \tag{20}$$

where y_{real} is the lagoon base temperature, $y_{approx.}$ is the nearby shallow lake and ANN simulated temperatures and $\bar{y}$ is the mean value of the data points. For a perfect approximation, $S_r = 0$ and $r = 1$, meaning that the approximated line fits all data points while $S_r = S_t$ and $r = 0$ denotes no improvement with respect to a straight line crossing the mean value.

The second criterion, which is widely used in many engineering applications, is the root mean square error (RMSE) defined as:

$$RMSE = \sqrt{\frac{\sum_{i=1}^{n} (y_{real} - y_{approx.})^2}{n}} \tag{21}$$

where the smaller values of RMSE imply smaller differences between the real data and approximated data. Table.1 represents the value of correlation coefficient (r) and RMSE for the shallow lake and ANN simulated temperatures.

Table. 1. Correlation coefficient (r) and RMSE of shallow lake temperatures and ANN simulated temperatures

Lorette

Lake	r	RMSE
Winnipeg Beach	0.938	2.875
Victoria Beach	0.928	3.086
Hecla Beach	0.918	3.215
Albert	0.942	2.779
Balsam	0.939	2.857
ANN	0.991	1.210

Niverville

Lake	r	RMSE
Gimli Beach	0.901	3.624
Grand Beach	0.915	3.367
Delta Beach	0.915	3.394
Grand Maraise	0.916	3.357
York Factory	0.503	9.711
ANN	0.997	0.907

Guelph

Lake	r	RMSE
Burlington Lake	0.901	3.177
Churry Beach	0.852	3.742
Cobourg Lake	0.858	3.823
Rideau Lake	0.880	3.640
Little C. Lake	0.861	4.083
ANN	0.998	0.418

Portage la Prairie

Lake	r	RMSE
Walker Lake	0.699	5.281
Playground Lake	0.758	4.814
Eleanor Lake	0.846	3.932
Dorothy Lake	0.846	3.938
Cross Lake	0.656	5.569
ANN	0.991	0.981

The maximum correlation coefficient (nearest to unity) in the nearby shallow lakes to Lorette, Niverville, Portage la Prairie and Guelph lagoons was 0.942, 0.916, 0.901 and 0.846, respectively. The smallest RMSE in the nearby shallow lakes to the four lagoons mentioned above was 2.779, 3.357, 3.177 and 3.932, respectively, meaning that significant discrepancies existed between the lagoon base and the nearby shallow lake temperatures. On the other hand, ANN-generated data points were of greater precisions. The correlation coefficient in data points generated by ANN was 0.991, 0.997, 0.998, and 0.991, in the Lorette, Niverville, Portage la Prairie and Guelph lagoons, respectively, very close to unity. RMSE in the data points of the four lagoons were 1.21, 0.907, 0.418 and 0.981, much less than those of the nearby shallow lake temperatures. In the light of the above, shallow lake temperatures are not suitable to use independently as sample lagoon base temperatures. However, if they first get processed by the ANN, they can be used as simulated lagoon temperatures.

ANN was then used once again to approximate the lagoon base temperature based on the corresponding air temperature. Five training methods including Levenberg-Marquardt (LM), Resilient Back-propagation (RBP), Fletcher-Powell Conjugate Gradient (FPCG), Polak-Ribiére Conjugate Gradient (PRCG), and Scaled Conjugate Gradient (SCG) were also used to compare the result of different training methods. To train the network, the currently existing lagoon temperatures (48 data points) and ANN-simulated lagoon temperatures (shallow lake temperatures processed with ANN) (192 data points) along with their corresponding air temperatures were fed into the network with10 hidden layers. The training/validation/test ratio of data points was 80/10/10 percent. Fig.7 illustrates the approximated result of each training approach. Also, the correlation coefficient and RMSE associated with each of the five training approaches are presented in Table.5.

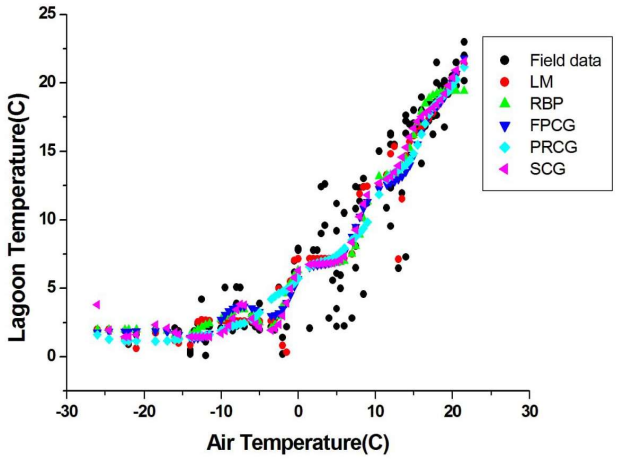

Fig. 7. Approximated lagoon temperature for different training approaches

Table. 2. Correlation factor and RMSE of the different training methods

Training approach	**Correlation factor (r)**	**RMSE**
Levenberg-Marquardt (LM)	0.9536	0.893
Resilient Back-propagation (RBP)	0.9468	0.929
Fletcher-Powell Conjugate Gradient (FPCG)	0.9493	0.912
Polak-Ribiére Conjugate Gradient (PRCG)	0.9515	0.899
Scaled Conjugate Gradient (SCG)	0.9456	0.943

It is clear that all five different approaches are close in their performances and differences are marginal. Levenberg-Marquardt has the closest correlation factor to unity (0.9536) and smallest RMSE value (0.893), thus provides the best fit for data points. This method was used as the selected method for the training of ANN in the following section.

3.4.7 Prediction of lagoon base temperature

According to the in situ measurements, the lagoon temperature reacts relatively slowly to any changes in air temperature, so that the mean monthly air temperature can provide adequate precision in the analysis. In this study, the future 50 years (2019-2069) mean monthly air temperatures were used for Faro, the nearest meteorological station, 60 kilometres west of Ross River, Yukon. The data were obtained from the CanESM2 climate model with three different pathways of rcp2.6, rcp4.5 and rcp8.5. These pathways consider different environmental variables such as precipitation, air pressure, cloud fraction, and wind speed for a location. A critical difference of nearly 8.6℃ exists in the maximum temperatures between the three climate projections while the difference in the minimum temperatures is smaller. The maximum and minimum projected air temperatures in the rcp2.6, rcp4.5, and rcp8.5 are 26.7, 30.1, 35.3℃, and -30.5, -32.9, and -29.3℃, respectively. As the rcp8.5 pathway provides higher temperatures, it was considered as the conservative case that relies on the hypothesis that if the GHE system can stabilize the permafrost at higher temperatures, it can preserve the icy layer at lower temperatures as well. Therefore, this pathway was selected and its predictions (Fig.8) were imported to the ANN as input data. Based on the analysis, the minimum and maximum lagoon temperatures are 0.28 ℃, and 22.52℃, respectively (Fig.9). This indicates that the lagoon base temperature is above zero-degree year-round, making it a constant heat source.

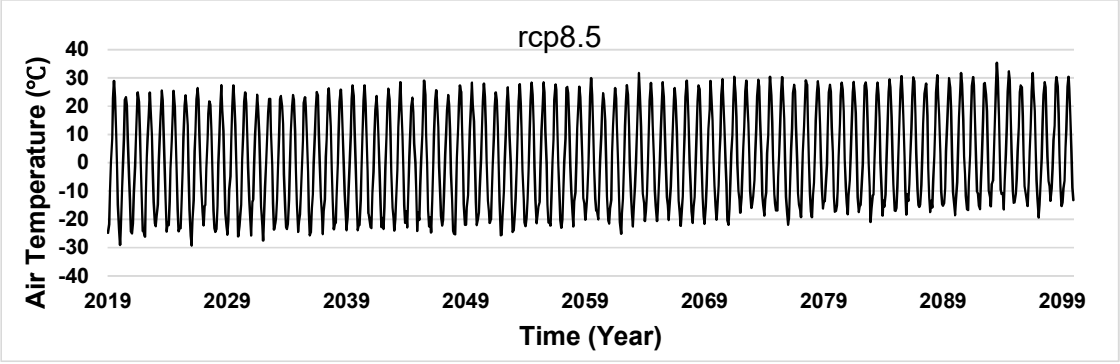

Fig. 8. Projection of monthly mean air temperature at Faro for CanESM2 rcp8.5 pathways (Environment and Climate Change Canada, 2020).

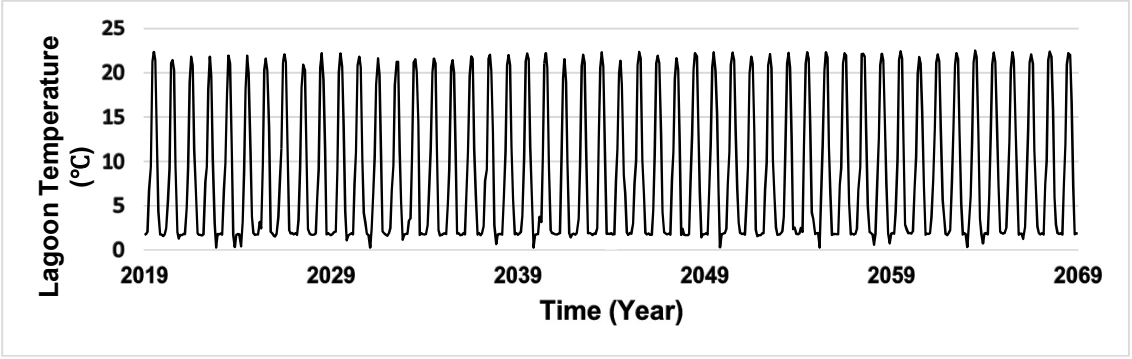

Fig. 9. ANN predicted future monthly lagoon base temperature based on forcing data from CanESM2, rcp8.5.

3.5 Numerical modelling and parameterization

3.5.1 Soil properties

Since no geotechnical laboratory tests have been conducted to determine the in-situ soil physical and thermal properties, average values for clay/sandy soils (Bergman et al., 2017) were considered as given in Table.3. Other parameters including water, ice, and coolant fluid thermal properties were taken from previous studies (Saaly et al., 2020; Côté & Konrad, 2005) . The required parameters for modelling the heat transfer in a porous matrix, thaw settlement and non-isothermal pipe flow are given in Table.4

Table. 3. Properties of the soils and fluids (Saaly et al., 2020; Bergman et al., 2017; Côté & Konrad, 2005)

Material	Thermal Conductivity [W/(m. K)]	Mass Heat Capacity [J/kg. K]	Density [kg/m^3]
Sandy Gravel	2.3	1255	2300
Clayey Silt	1.25	942	1900
Water	0.56	4188	1000
Ice	2.2	2093	917
30% Ethanol-water blend	0.41	4250	955

Table. 4. Parameters used for heat transfer and isothermal pipe flow (Bergman et al., 2017; Tsytovich, 1985)

Property	**Value**
Latent heat of water (L_f) [kJ/kg]	334
Phase change temperature (T_{pc}) [°C]	0
Upward heat flux[1] [W/m^2]	0.075
Friction model	Churchill
HDPE pipe surface roughness [mm]	0.0015
HDPE pipe wall thickness [mm]	2
HDPE pipe wall thermal conductivity [W/(m. K)]	0.46
Residual unfrozen volumetric water content (θ_{wr})	0.058
Thaw strain of frozen soil (δ)	0.1
Thaw compression coefficient of frozen soil (α) [1/MPa]	0.75
Volumetric compression coefficient (m_v) [1/MPa]	0.3

[1] Geothermal Maps of Canada (Grasby et al., 2009)

3.5.2 Mesh

The triangular Lagrange finite elements were applied for the heat transfer and non-isothermal pipe models (Liu, et al., 2019). The mesh consistency testing showed that the nodal distance associated with “extra fine” mesh in COMSOL Multiphysics resulted in consistent results even if a smaller nodal distance was selected (Fig.10). Also, “extremely fine” meshing was assigned to the area close to the lagoon base and GHEs to increase the precision in the analysis.

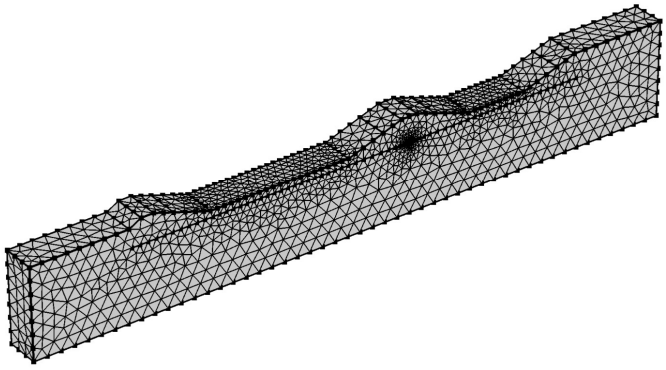

Fig. 10. Domain mesh configuration

Chapter 4: Results and Discussions

4.1.1 Model validation

To validate the subsurface temperature distribution and reach a state of equilibrium, 175 days were initially defined as the first phase. This phase was chosen from 29 Nov 2018 to 24 May 2019 where the ground temperatures were available from the two borehole tests of BH18-05 and BH18-06. During this period no heat pump system operated and the temperature distribution only from the surface climatic heat flux at the top and bottom of the domain was studied. The climatic parameters for modelling the heat flux were the upward heat flux, air temperature and wind speed obtained from Environment and Climate Change Canada (2020, station Faro). Following the first phase, the operation phase proceeded for 50 years (from May 2019 to May 2069) such that its initial ground temperature was the ground temperature at the end of the first phase (24 May 2019).

The maximum differences in the temperature profile between the field measurement and numerical modelling are 0.1°C (at the depth of 2.11 m) and 2.2°C (at the depth of 1.93 m) in BH18-05 and BH18-06, respectively (Fig.11). This difference is probably due to the small difference in the climatic parameters between Ross River and those of Faro used as the nearest station to the site. Despite the marginal differences in the near ground temperature, the finite element modelling could properly simulate the deeper subsurface temperature where the permafrost exists.

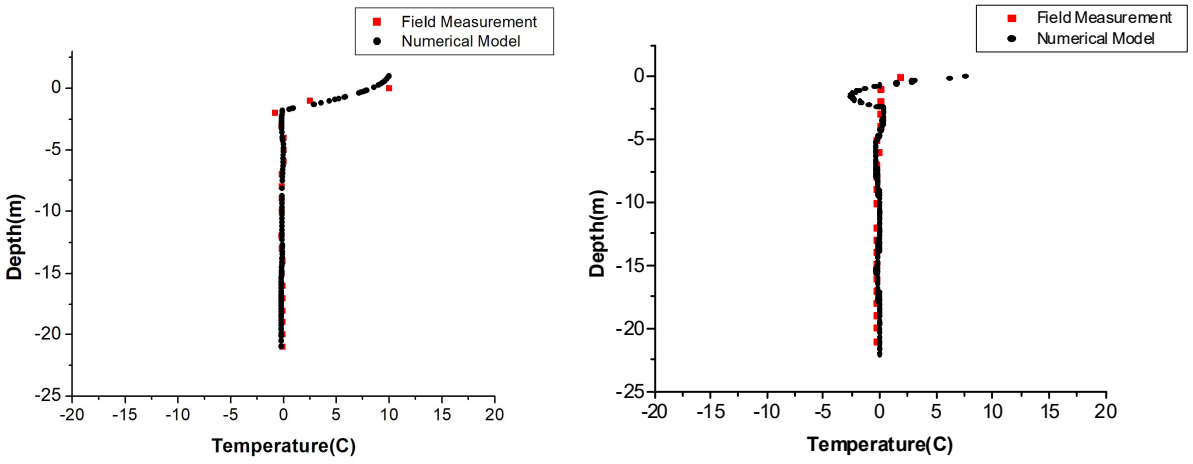

BH18-05 BH18-06

Fig. 11. Simulated and observed ground temperature profile for boreholes BH18-05 and BH18-06 on 24 May, 2019

4.1.2 Effect of GHE system on permafrost preservation

The maximum annual isothermal contours in the central cut plane (cut plane A-A illustrated in Fig.12) and in the 0 (2019), 1st (2020), 5th (2024), 10th (2029), 25th (2044), and 50th (2069) years (Fig.10) from the finite element simulation reveals that the permafrost table significantly varied over the 50-year study time due to the climatic and lagoon heat fluxes. The onset of permafrost thawing was the first year, where the permafrost below the lagoon (along the cut line A-A) thawed by an average of 0.45 m by the end of 2020. The permafrost thawing depth below the lagoon continued to increase in the following years, reaching 4.52 m and 7.68 m in 2024 and 2029, respectively. The entire permafrost completely thawed after 17 years (2036) and the maximum temperature of the thawed permafrost area reached 5.5°C and 7°C (both at the depth of 14 m) in 2044 and 2069, respectively (Fig.13a).

The foundation permafrost thawed faster beneath the lagoon compared to the embankment. The permafrost thaw depth below the embankment (along the cut line B-B) in 2024 and 2029 was 2.32 m and 3.57 m, respectively, which were 2.20 m and 4.11 m less than that of permafrost underneath the lagoon at the corresponding years. Unlike the embankment, the lagoon never experienced negative temperatures and produced a constant heat flux, so the permafrost under the lagoon was more prone to thawing.

Thaw settlement, as the name suggests, only takes into account the settlement due to the permafrost thawing so it only continues until there is no permafrost left. The thaw settlement beneath the wastewater lagoon was 1.0 cm in 2020 and reached 1.57 m in 2036 when the entire permafrost thawed. Thaw settlement beneath the embankment, on the other hand, was 6.0 cm in 2021 and reached 1.72 m in 2045. The maximum difference in the settlement under the lagoon and the embankment was 92 cm in 2036, a considerable number that can contribute to significant damages to the dikes due to the uneven settlement.

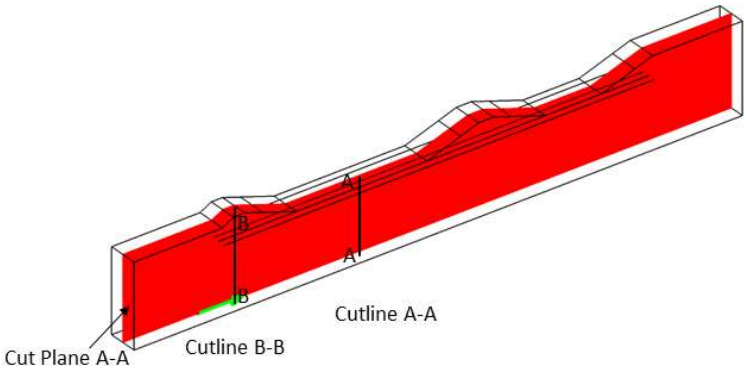

Fig. 12. The defined cut lines and cut plane

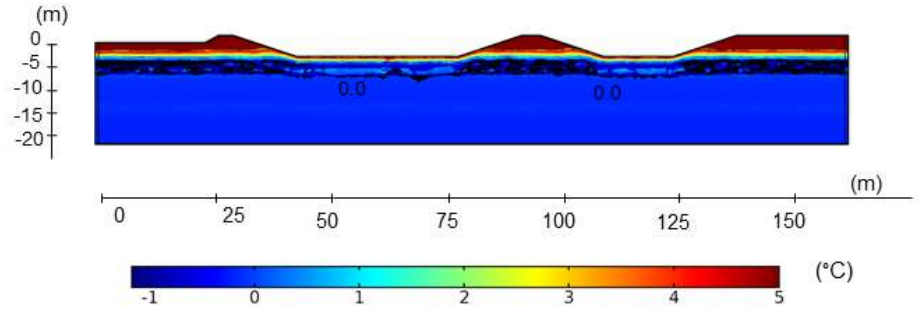

2019

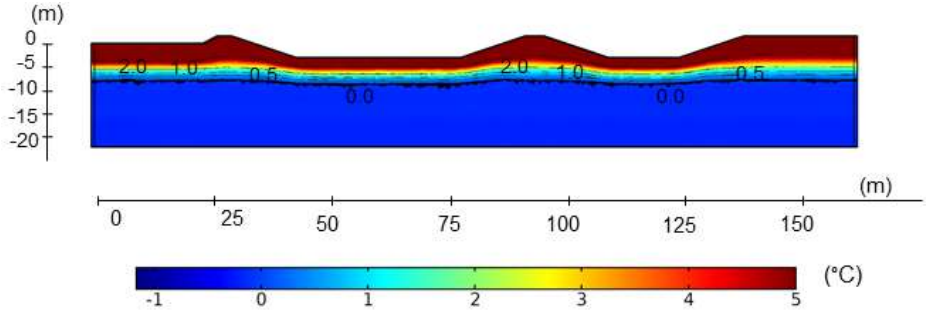

2020

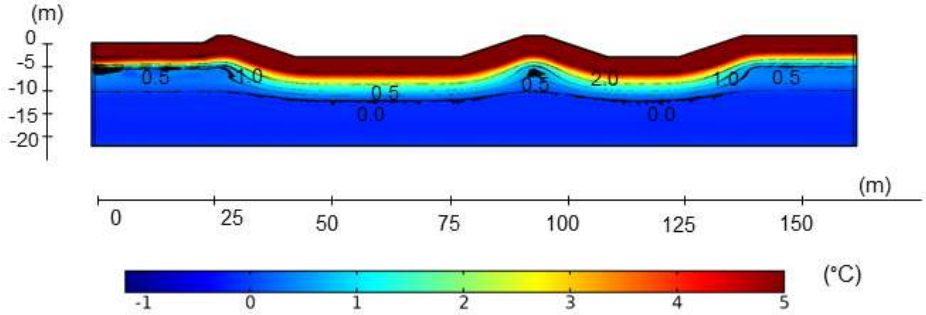

2024

(continued)

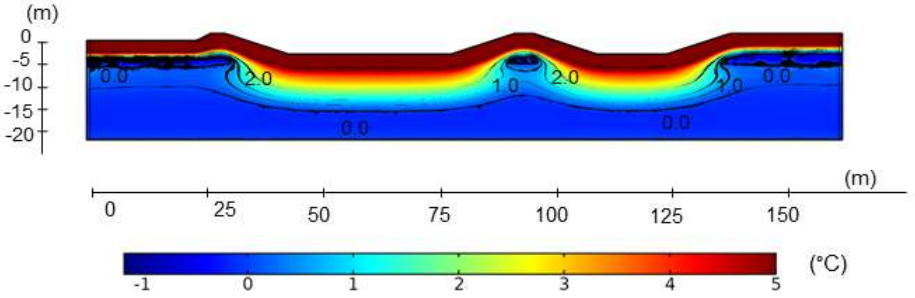

2029

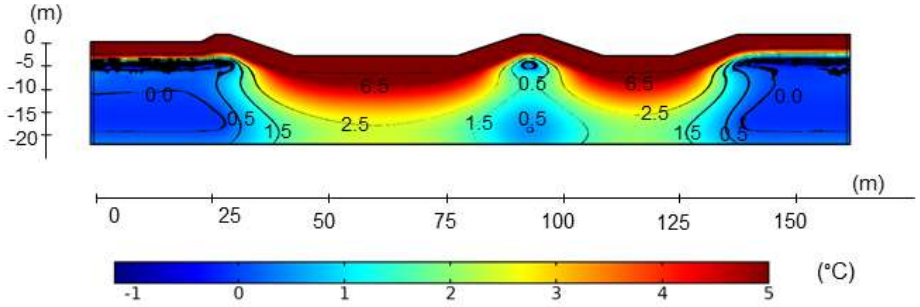

2044

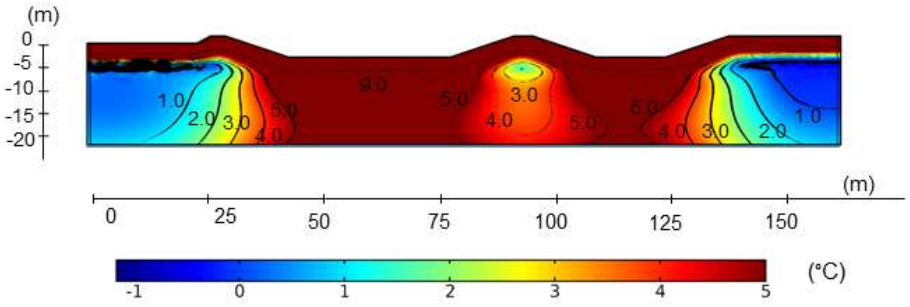

2069

Fig. 13. Maximum annual temperature (°C) in cut plane A-A without GHE system in six different years

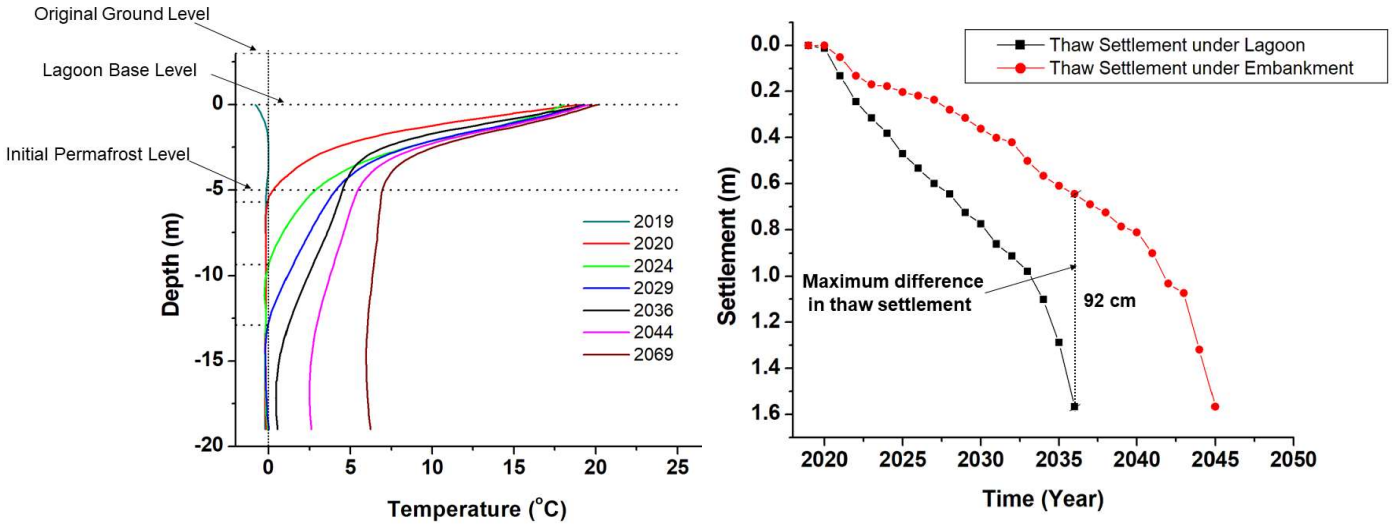

(a) (b)

Fig. 14. a) Temperature profile and permafrost thaw depth along the cut line A-A and b) lagoon and embankment settlement due to the permafrost thaw and with no embedded GHE system

HDPE heat exchangers were embedded within the domain to see the effect of GHEs on permafrost stabilization. The short-term and long-term temperature variation in the cut plane A-A with the embedded GHE system was studied as isothermal contours of maximum annual temperature in 2019, 2020, 2024, 2029, 2044, and 2069 (Fig.15). Also, the temperature variation along the cut line A-A at the mentioned times and the thaw settlement values over 50 years are given in Fig. 16a and 16b, respectively.

The GHE system proved to be capable of preventing permafrost thaw in all permafrost areas in the short-term (up to 10 years) where the warmest permafrost section in 2020, 2024, and 2029 was at the bottom of the domain with a temperature of -0.12, -0.05 and -0.03°C, respectively. However, in the long-term, the bottom permafrost started to thaw as its temperature continued to rise. The permafrost thawing from the bottom means that in the long-term, the existing geothermal heat flux at the site outweighed the freezing effect of the GHE system. The thaw depth of the permafrost bottom under the lagoon was 2.81 m (19.6% of the entire permafrost cross-section) in 2044 and 3.02 m (20.3% of the entire permafrost cross-section) in 2069. These values were 2.61 m and 2.33 m under the embankment. Therefore, the maximum thaw settlement under the lagoon and embankment after 50 years was 51.0 cm and 53.0 cm, respectively. Also, the maximum difference in the thaw settlement below the lagoon and the embankment was 5.0 cm and in 2048, a 94.5% reduction compared with no operational GHEs scenario.

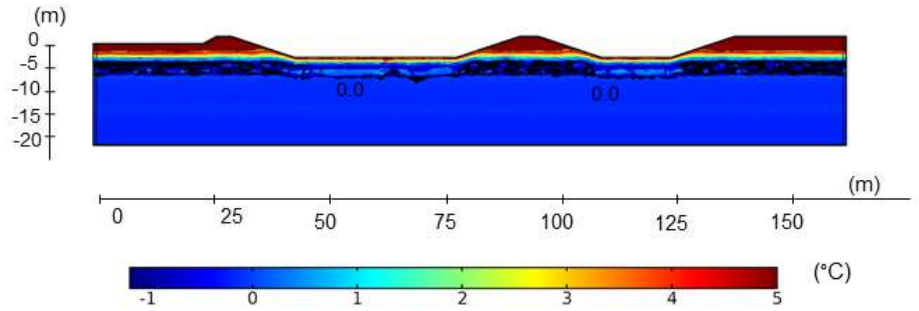

2019

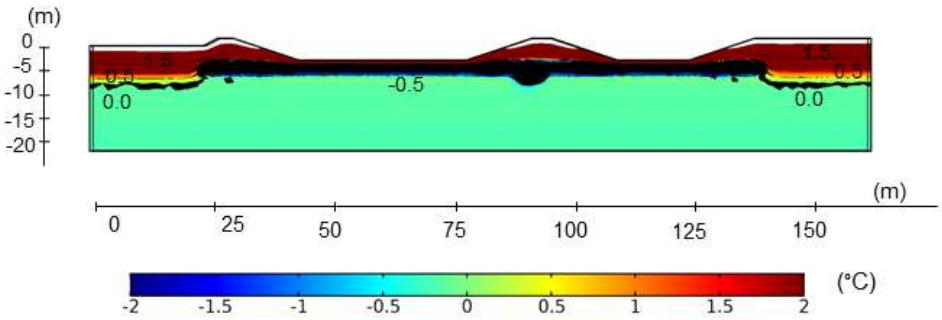

2020

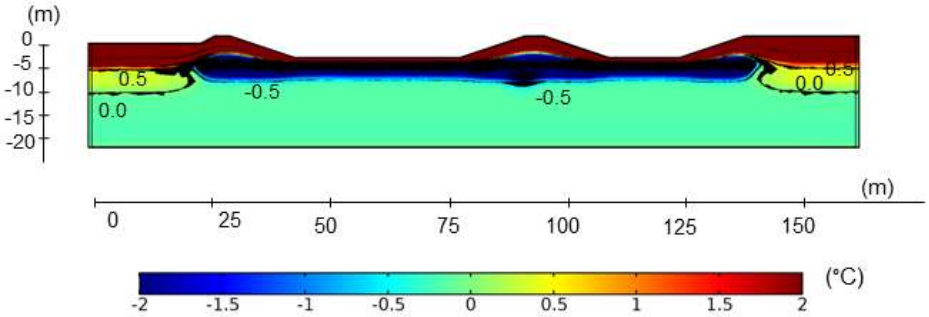

2024

(continued)

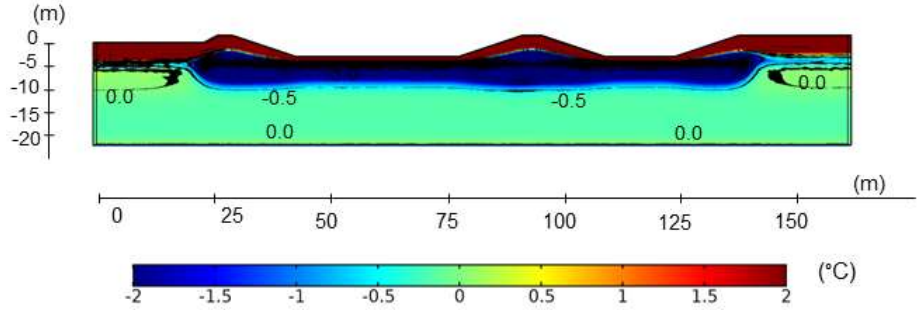

2029

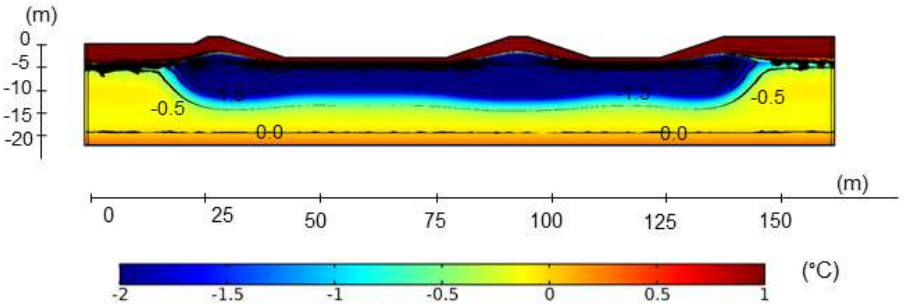

2044

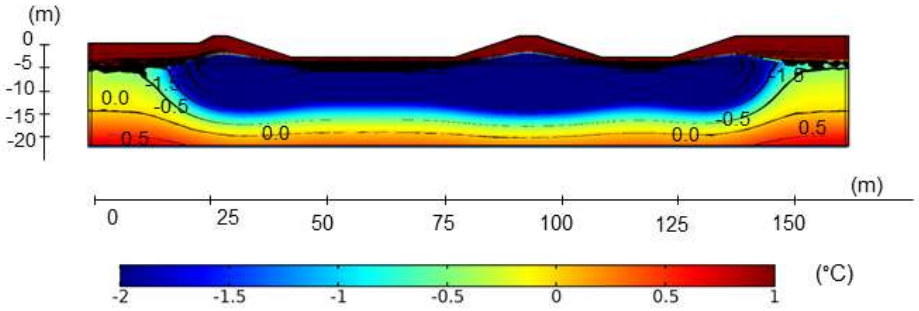

2069

Fig. 15. Maximum temperature (°C) in cut plane A-A equipped with the GHE system in six different years

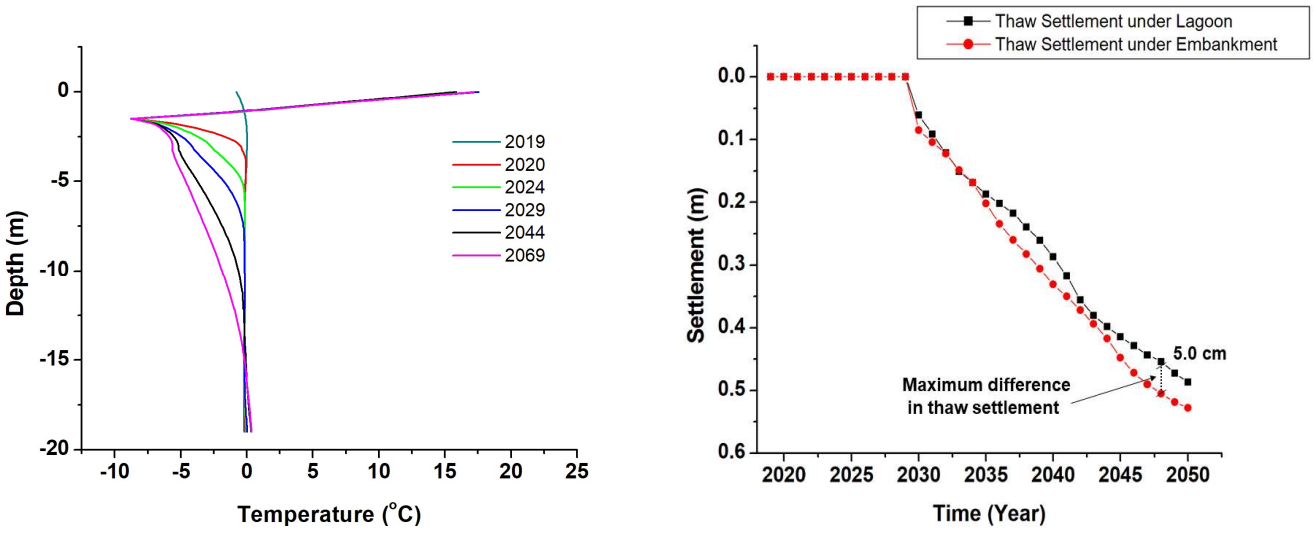

Fig. 16. a) Temperature profile along cut line A-A at different times and b) lagoon and embankment settlements due to the permafrost thaw in the presense of embeded GHE system

4.1.3 The effect of operational parameters on the GHE performance

Analyzing different operational parameters given in Table.5 proved that they have a significant impact on the thawed permafrost thicknesses. All the permafrost thawing was from the bottom while the upper permafrost areas stayed intact throughout the 50-year study period. The first studied parameter was pipe spacing. Studying this parameter revealed that pipe spacing does not considerably affect permafrost thaw depth in the first half of the study period. All three different pipe spacings resulted in 0, 0, and 0.21 m thaw thickness in 2020, 2024, and 2029 and only up to 3-cm difference in the thaw thickness was observed for the different pipe spacings in 2044. In the long-term, on the other hand, closer pipe configurations (more pipes) resulted in smaller thawed permafrost thickness since the effective radial distance (i.e. where the GHEs maintain the soil temperature in a frozen state) of closer GHEs grew enough such that they overlapped with the adjacent pipes' effective radial distance, resulted in blocking the lagoon heat from reaching the permafrost (Fig.17). In comparison with 1 m pipe spacing, 1.5, 2, and 2.5 m pipe spacings resulted in 10.1%, 26.5%, and 46.0% increases in the thaw thickness in the second half of the study period, respectively.

Compared to 1 m pipe spacing, the final thaw settlement under the lagoon rose by 10.0%, 23.3% and 40.0% in pipes with 1.5, 2, and 2.5 m spacing, respectively. Despite the delay in triggering and decrease in the permafrost thawing, pipes with all four spacings failed to eliminate permafrost thawing over 50 years.

Table. 5. The effect of operational parameters on the permafrost thaw depth and settlement

Operational Parameter	Value	Permafrost Thaw Depth (m)					Final Thaw Settlement (m)
		2020	2024	2029	2044	2069	
Pipe Spacing (m)	1	0	0	0.21	2.82	4.11	0.60
	1.5	0	0	0.21	2.84	4.57	0.66
	2.0	0	0	0.21	2.85	5.20	0.74
	2.5	0	0	0.21	2.85	6.00	0.84
Fluid Velocity (m/s)	0.2	0	0	0.21	2.85	6.00	0.84
	0.4	0	0	0.21	2.85	5.85	0.82
	0.6	0	0	0.21	2.84	5.80	0.81
Fluid Temperature (°C)	-5	0	0	0.21	2.85	6.00	0.84
	-10	0	0	0.21	2.75	3.60	0.53
	-15	0	0	0.21	2.60	1.86	0.29
	-20	0	0	0.21	2.44	0.26	0.04

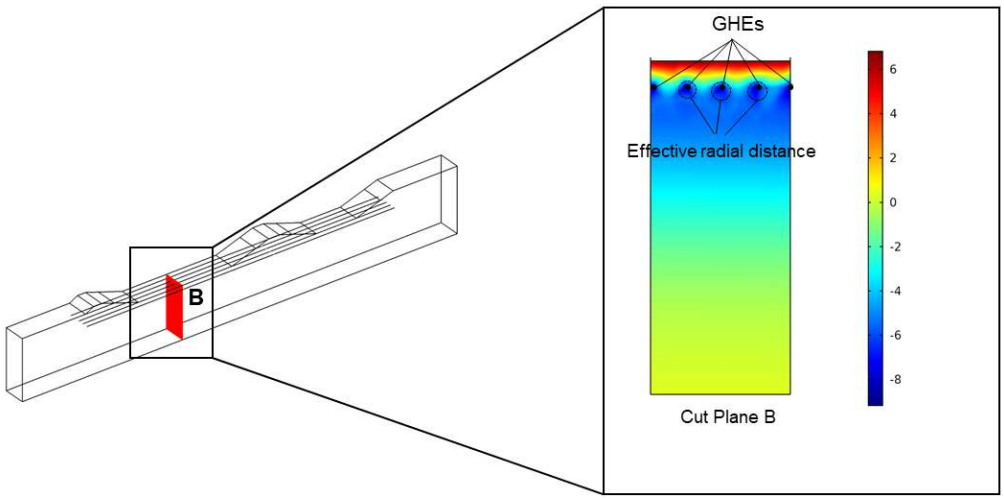

Fig. 17. The effective radial distance of GHEs and the soil temperature (°C) profile of the cut plane B

The inlet velocities did not contribute to any changes in the thawed permafrost thickness in the short-term. All three different velocities resulted in 0, 0 and 0.21 m thaw thickness in 2020, 2024, and 2029, respectively. In 2044, the thaw thickness was only 1 cm smaller for faster fluid inlet velocity. However, between 2044 and 2069, the fluid inlet velocity caused a greater difference in the thawed permafrost thickness where compared to using the 0.2 m/s fluid inlet velocity, the 0.4 m/s and 0.6 m/s fluid inlet velocities resulted in 2.5 % and 3.3% reduction in the thawed permafrost thickness, respectively. The probable explanation for the reduction in thawed permafrost thickness is that a faster heat carrier passes

the domain in a shorter time, so it loses the cold much less. Therefore, the passing fluid stays cold enough along the system to freeze back the permafrost. Also, similar to pipe spacing variation, all three inlet velocities failed to prevent permafrost thawing.

The inlet temperature played a substantial role in the permafrost level, such that, unsurprisingly, cooler fluids resulted in less permafrost thaw since according to Fourier's law (Eq.2), a larger temperature differential (gradient) between the GHE system and the ambient soil leads to the greater transferred (extracted) heat.

All the fluid inlet temperatures led to a delay in triggering permafrost thaw; however, none eliminated the permafrost thaw. During the 50-year lifespan of the system and by using -5°C fluid temperature, 42.6% of permafrost cross-section thawed, while this number was 25.7%, 13.3%, and 1.9% for fluid temperatures of -10, -15, and -20°C, respectively. Compared to using -5°C fluid temperature, the thaw settlement at the end of this period decreased by 36.9%, 65.5%, and 95.2% for the fluid inlet temperatures of -10, -15, and -20°C, respectively.

Up to 2029, the fluid inlet temperature did not make any difference in the thawed permafrost thickness, where all four temperatures resulted in 0.21 m thaw thickness. Following that, the variation in the thaw thickness due to the different fluid temperatures took place. In 2044 and compared with an inlet temperature of -5°C, by using fluid inlet temperatures of -10, -15, and -20°C, the permafrost thaw thickness was reduced by 3.5%, 8.8% and, 14.4%, respectively. The reduction in 2069 was 40.0%, 69.0%, and 95.7%, for fluid inlet temperatures of -10, -15 and, -20°C, respectively, meaning that the effect of fluid inlet temperature on the thaw thickness is more significant after 25 years of the GHE operation. The main reason is that in the long-term, the cold fluid temperatures have enough time to produce a big effective radial distance such that they overlap with the adjacent pipes' radial distance, resulting in blocking the lagoon heat from reaching the permafrost.

Chapter 5: Conclusion and Recommendations for Future Work

This thesis investigated the long-term performance of the GHE system and the effect of some of its operational parameters on permafrost stabilization. The study site was located in a wastewater lagoon facility in Ross River, Yukon, Canada where the huge heat leakage in a conventional lagoon was expected to induce permafrost degradation and significant thaw settlement. The proposed GHE system consisted of horizontal closed-looped high-density polyethylene pipes buried below the wastewater lagoon. To study the long-term performance of the GHE system on preserving permafrost beneath the lagoon, the future lagoon base temperature was obtained by a data-driven artificial neural network. Due to the inadequate available lagoon base temperatures, the bottom temperature of several shallow lakes with similar temperatures to the lagoon base temperature was fed to the neural network as well.

The results illustrated that the entire permafrost would thaw after seventeen years under the climatic and lagoon heat fluxes. The thaw rate was more notable under the lagoon in the long-term, resulting in an uneven settlement in the subsurface. Also, due to the considerable constant upward geothermal heat flux at the bottom boundary, the GHE system could not eliminate the permafrost degradation and thus thaw settlement beneath the wastewater lagoon during its lifespan. However, the heat exchangers could significantly mitigate and postpone the permafrost thawing.

Additionally, the heat exchangers' operational parameters proved to substantially affect the permafrost thaw thickness. The most influential parameter was the heat exchanger fluid temperature. On the other hand, the fluid inlet velocity only made small differences in the thaw depth and thaw settlement. Also, the fluid inlet temperature and pipe spacing are more influential on the permafrost thaw in the long-term.

It should be noted that although the simulation can evaluate and predict the future GHE system performance, there are some levels of uncertainty associated with the projected climate data and lagoon base temperature used in this study. However, the worst-case climate scenario used herein provided safety levels that can compensate for uncertainties in data. It is also necessary to mention that the GHE system could stabilize the upper zone of permafrost immediately underneath the Ross River wastewater lagoon. However, besides the operational parameters discussed here, the GHE performance depends on the permafrost elevation and temperature, soil stratigraphy, and thermal properties. Also, the effect of the burial depth of the GHEs should be investigated. In light of the above, more case studies are needed to increase the results' reliability. It is suggested that the lagoon base temperatures be monitored year-round to generate more reliable future lagoon base temperatures. In addition, thaw settlement is a multiphysical process that involves thermal, hydraulic, and mathematical fields interacting with each

other; therefore, to be addressed properly, it requires a constitutive model that integrates the above-mentioned physics.

References

Al-Khoury, R. (2011). *Computational modeling of shallow geothermal systems*. CRC press.

Bayasan, R. M., Korotchenko, A. G., Volkov, N. G., Pustovoit, G. P., & Lobanov, A. D. (2008). Use of two-phase heat pipes with the enlarged heat-exchange surface for thermal stabilization of permafrost soils at the bases of structures. *Applied Thermal Engineering, 28*(4), 274-277.

Bemister, A. E. (1978). Cold temperature bio-kinetics of aerated lagoons.

Bergman, T. L., Lavine, A., Incropera, F. P., & Dewitt, D. P. (2017). *Fundamentals of heat and mass transfer*. John Wiley & Sons New York.

Cai, W., Wang, F., Liu, J., Wang, Z., & Ma, Z. (2019). Experimental and numerical investigation of heat transfer performance and sustainability of deep borehole heat exchangers coupled with ground source heat pump systems. *Applied Thermal Engineering, 149*, 975-986.

Chiasson, A. D. (2016). *Geothermal heat pump and heat engine systems: Theory and practice*. John Wiley & Sons.

Claesson, J., & Dunand, A. (1983). Heat extraction from ground by horizontal pipes. Swedish Council of building Research. *Document D1*.

Côté, J., & Konrad, J.-M. (2005). A generalized thermal conductivity model for soils and construction materials. *Canadian Geotechnical Journal, 42*(2), 443-458.

Dacquay, C., Holländer, H. M., Kavgic, M., Maghoul, P., Liu, H., & Fujii, H. (2020). Evaluation of an integrated sewage pipe with ground heat exchanger for long-term efficiency estimation. *Geothermics, 86*, 101796.

Dijkshoorn, L., Speer, S., & Pechnig, R. (2013). Measurements and design calculations for a deep coaxial borehole heat exchanger in Aachen, Germany. *International Journal of Geophysics, 2013*.

Doré, G., Niu, F., & Brooks, H. (2016). Adaptation methods for transportation infrastructure built on degrading permafrost. *Permafrost and Periglacial Processes, 27*(4), 352-364.

Florides, G., & Kalogirou, S. (2007). Ground heat exchangers—A review of systems, models and applications. *Renewable Energy, 32*(15), 2461-2478.

Florides, G. A., Christodoulides, P., & Pouloupatis, P. (2013). Single and double U-tube ground heat exchangers in multiple-layer substrates. *Applied energy, 102*, 364-373.

Fontaine, P.-O., Marcotte, D., Pasquier, P., & Thibodeau, D. (2011). Modeling of horizontal geoexchange systems for building heating and permafrost stabilization. *Geothermics, 40*(3), 211-220.

Gauthier, C., Lacroix, M., & Bernier, H. (1997). Numerical simulation of soil heat exchanger-storage systems for greenhouses. *Solar energy, 60*(6), 333-346.

Gheysari, A. F., Holländer, H. M., Maghoul, P., & Shalaby, A. (2021). Sustainability, climate resiliency, and mitigation capacity of geothermal heat pump systems in cold regions. *Geothermics, 91*, 101979.

GISTEMP Team, G. S. T. A. G., version 4. NASA Goddard Institute for Space Studies. Dataset accessed 2021-01-25 at https://data.giss.nasa.gov/gistemp/.

Gregersen, O., Phukan, A., & Johansen, T. (1985). Engineering properties and foundation design alternatives in marine Svea clay, Svalbard. *Publikasjon-Norges Geotekniske Institutt*(159), 1-5.

Hart, O. E., & Halden, R. U. (2020). Modeling wastewater temperature and attenuation of sewage-borne biomarkers globally. *Water research, 172*, 115473.

Heginbottom, J., Dubreuil, M., & Harker, P. (1995). Canada, Permafrost. National Atlas of Canada. *Natural Resources Canada, 5th Edition, MCR, 4177*.

Holubec, I. (2008). Flat Loop Thermosyphon Foundations in Warm Permafrost, Northwest Territories Public Works and Services.

Huang, B., Lee, J., & Chyng, J. (2005). Heat-pipe enhanced solar-assisted heat pump water heater. *Solar Energy, 78*(3), 375-381.

Jiao, B., Qiu, L., Zhang, X., & Zhang, Y. (2008). Investigation on the effect of filling ratio on the steady-state heat transfer performance of a vertical two-phase closed thermosyphon. *Applied Thermal Engineering, 28*(11-12), 1417-1426.

Kayaci, N., & Demir, H. (2018). Long time performance analysis of ground source heat pump for space heating and cooling applications based on thermo-economic optimization criteria. *Energy and Buildings, 163*, 121-139.

Kayaci, N., Demir, H., Atayılmaz, Ş. Ö., & Ağra, Ö. (2015). Long Term Simulation of Horizontal Ground Heat Exchanger for Ground Source Heat Pump. ASME International Mechanical Engineering Congress and Exposition,

Ladanyi, B., & Andersland, O. (2004). *Frozen ground engineering*. Wiley.

Lamarche, L. (2019). Horizontal ground heat exchangers modelling. *Applied Thermal Engineering, 155*, 534-545.

Lewkowicz, A. G., & Way, R. G. (2019). Extremes of summer climate trigger thousands of thermokarst landslides in a High Arctic environment. *Nature communications, 10*(1), 1-11.

Liu, H., Maghoul, P., Bahari, A., & Kavgic, M. (2019). Feasibility study of snow melting system for bridge decks using geothermal energy piles integrated with heat pump in Canada. *Renewable Energy, 136*, 1266-1280.

Liu, H., Maghoul, P., Shalaby, A., & Bahari, A. (2019). Thermo-hydro-mechanical modeling of frost heave using the theory of poroelasticity for frost-susceptible soils in double-barrel culvert sites. *Transportation Geotechnics, 20*, 100251.

Mei, V. C. (1991). Heat transfer of buried pipe for heat pump application.

Michalowski, R., & Zhu, M. (2004). Constitutive model for heaving of frost susceptible soils. Numerical Models in Geomechanics: Proceedings of the Ninth International Symposium on'Numerical Models in Geomechanics-NUMOG IX', Ottawa, Canada,

Oleszkiewicz, J., & Sparling, A. (1987). Wastewater lagoons in a cold climate. *Water science and technology, 19*(12), 47-53.

Omer, A. M. (2008). Ground-source heat pumps systems and applications. *Renewable and sustainable energy reviews, 12*(2), 344-371.

Saaly, M., Bobko, K., Maghoul, P., Kavgic, M., & Holländer, H. (2020). Energy performance of below-grade envelope of an institutional building in cold regions. *Journal of Building Engineering, 27*, 100911.

Saaly, M., Maghoul, P., Kavgic, M., & Polyzois, D. (2019). Performance analysis of a proposed geothermal pile system for heating and cooling energy demand for a building in cold regions. *Sustainable Cities and Society, 45*, 669-682.

Saaly, M., Sinclair, R., Kurz, D., Maghoul, P., Holländer, H., & Gheisari, A. F. (2020). Assessment of a Closed-Loop Geothermal System for Seasonal Freeze-Back Stabilization of Permafrost, GeoVirtual, 2020

Schuur, E. A., McGuire, A. D., Schädel, C., Grosse, G., Harden, J., Hayes, D. J., Hugelius, G., Koven, C. D., Kuhry, P., & Lawrence, D. M. (2015). Climate change and the permafrost carbon feedback. *Nature, 520*(7546), 171-179.

Self, S. J., Reddy, B. V., & Rosen, M. A. (2013). Geothermal heat pump systems: Status review and comparison with other heating options. *Applied energy, 101*, 341-348.

Sinclair, R., and Kenton Theissen. (2014). Ross River wastewater treatment system, Ross River, Yukon. Final design report, Winnipeg: KGS Group.

Smyth, K., Vendramelli, R., Dankewich, D., & Yuan, Q. (2018). Seasonal variations in cold climate nutrient removal: A comparison of facultative and aerated lagoons. *Journal of environmental management, 214*, 224-231.

Tetra Tech, EBA. "Geothermal Evaluation-Proposed Wastewater Disposal Facilities, Ross River, YT.". (2014).

Subcommittee, P. (1988). Glossary of permafrost and related ground-ice terms. *Associate Committee on Geotechnical Research, National Research Council of Canada, Ottawa, 156*.

Tsytovich, H. (1985). Mechanics of frozen soil, Science Press, Beijing (In Chinese, Translated by Zhang CQ and Zhu YL).

Vyalov, C. (2005). Rheology of frozen soil (translated by Liu jK et al.). *China Railway Science Press, Beijing*, 135-137.

Welty, J., Rorrer, G. L., & Foster, D. G. (2020). *Fundamentals of momentum, heat, and mass transfer*. John Wiley & Sons.

Wen, Z., Sheng, Y., Ma, W., & Qi, J. (2008). In situ experimental study on thermal protection effects of the insulation method on warm permafrost. *Cold Regions Science and Technology, 53*(3), 369-381.

Wu, Z., Zhang, J., & Zhu, Y. (1983). Field experiments creep of ground ice on Qinghai-Xizang Plateau. *Professional Papers on Permafrost Studies of Qinghai-Xizang Plateau. Academia Sinica, Lanzhou, China*, 120-123.

Yoon, S., Lee, S.-R., & Go, G.-H. (2015). Evaluation of thermal efficiency in different types of horizontal ground heat exchangers. *Energy and Buildings, 105*, 100-105.

Zhang, J., Ruan, G., Su, K., & Zhang, H. (2016). Estimation on settlement of precast tower footings along the Qinghai–Tibet Power Transmission Line in warm permafrost regions. *Cold Regions Science and Technology, 121*, 275-281.

Zhang, M., Zhang, J., & Lai, Y. (2005). Numerical analysis for critical height of railway embankment in permafrost regions of Qinghai–Tibetan plateau. *Cold Regions Science and Technology, 41*(2), 111-120.

Zhi, W., Yu, S., Wei, M., Jilin, Q., & Wu, J. (2005). Analysis on effect of permafrost protection by two-phase closed thermosyphon and insulation jointly in permafrost regions. *Cold Regions Science and Technology, 43*(3), 150-163.